Cell Reports

Article

MicroRNA miR-29c regulates RAG1 expression and modulates V(D)J recombination during B cell development

Graphical abstract

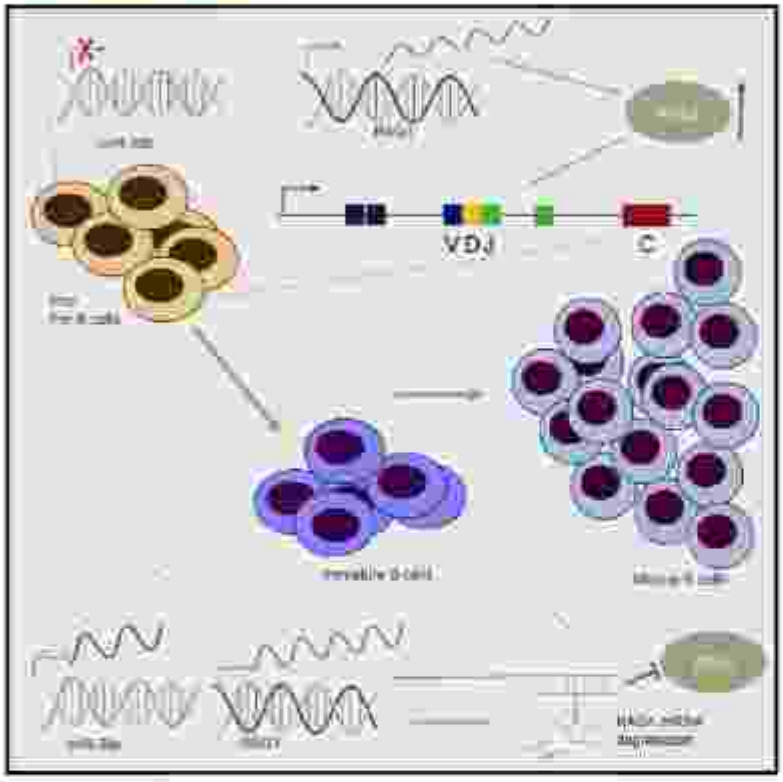

Authors

Rupa Kumari, Urbi Roy, Sagar Desai, ..., Adrian Liston, Bibha Choudhary, Sathees C. Raghavan

Correspondence

vibha@ibab.ac.in (B.C.), sathees@iisc.ac.in (S.C.R.)

In brief

Kumari et al. report that miR-29c is a negative regulator of RAG1 in B cells of mice and humans. Overexpression of miR-29c reduces V(D)J recombination, while its quenching increases the efficiency of recombination. miR-29c holds potential as a biomarker and in cancer therapeutics.

Highlights

- miR-29c regulates RAG1 expression in mice and humans
- miR-29c modulates V(D)J recombination in pre-B cells by regulating RAG1 expression
- miR-29c and Rag1 expression are inversely correlated in developing B cells in mice
- Leukemia patients show a negative correlation for expression of miR-29c and RAG1

Kumari et al., 2021, Cell Reports 35, 109390
July 13, 2021
https://doi.org/10.1016/j.celrep.2021.109390

CellPress

Cell Reports

CellPress
OPEN ACCESS

Article

MicroRNA miR-29c regulates RAG1 expression and modulates V(D)J recombination during B cell development

Rupa Kumari,[1,9] Urbi Roy,[1,9] Sagar Desai,[2,3,10] Namrata M. Nilavar,[1,10] Annemarie Van Nieuwenhuijze,[4] Amita Paranjape,[5] Gudapureddy Radha,[1] Pushpinder Bawa,[6] Mrinal Srivastava,[6] Mridula Nambiar,[6] Kithiganahalli Narayanaswamy Balaji,[7] Adrian Liston,[4] Bibha Choudhary,[2,7,*] and Sathees C. Raghavan[1,11,12,*]

[1]Department of Biochemistry, Indian Institute of Science, Bangalore 560012, India
[2]Institute of Bioinformatics and Applied Biotechnology, Bangalore 560100, India
[3]Manipal Academy of Higher Education, Manipal, Karnataka 576104, India
[4]Department of Microbiology and Immunology, Laboratory of Adaptive Immunity, KU Leuven, Leuven, Belgium
[5]TIFR Centre for Interdisciplinary Sciences, Tata Institute of Fundamental Research (TIFR), Hyderabad 500046, India
[6]Department of Biology, Indian Institute of Science Education and Research, Pune, India
[7]Department of Microbiology and Cell Biology, Indian Institute of Science, Bangalore 560012, India
[8]Immunology Programme, Babraham Institute, Cambridge, United Kingdom
[9]These authors contributed equally
[10]These authors contributed equally
[11]Senior author
[12]Lead contact
*Correspondence: [redacted] (B.C.), [redacted] (S.C.R.)
https://doi.org/10.1016/j.celrep.2021.109390

SUMMARY

Recombination activating genes (RAGs), consisting of RAG1 and RAG2, are stringently regulated lymphoid-specific genes, which initiate V(D)J recombination in developing lymphocytes. We report the regulation of RAG1 through a microRNA (miRNA), miR-29c, in a B cell stage-specific manner in mice and humans. Various lines of experimentation, including CRISPR-Cas9 genome editing, demonstrate the target specificity and direct interaction of miR-29c to RAG1. Modulation of miR-29c levels leads to change in V(D)J recombination efficiency in pre-B cells. The miR-29c expression is inversely proportional to RAG1 in a B cell developmental stage-specific manner, and miR-29c null mice exhibit a reduction in mature B cells. A negative correlation of miR-29c and RAG1 levels is also observed in leukemia patients, suggesting the potential use of miR-29c as a biomarker and a therapeutic target. Thus, our results reveal the role of miRNA in the regulation of RAG1 and its relevance in cancer.

INTRODUCTION

Recombination activating genes (RAGs), comprising lymphoid-specific proteins, RAG1 and RAG2, initiate V(D)J recombination, a process by which antigen receptor diversity is generated (Gellert, 2002; Schatz and Swanson, 2011). Immunoglobulin (Ig) and T cell receptor genes are assembled from variable (V), diversity (D), and joining (J) gene segments during the development of lymphocytes (Gellert, 2002; Nishana and Raghavan, 2012). DNA binding and cleavage by RAGs occur at specific sequences called recombination signal sequences (RSSs) that flank each of the V, D, and J segments (Schatz and Ji, 2011). Each RSS consists of conserved heptamer and nonamer, along with a less conserved spacer sequence of 12 or 23 bp (termed as 12 or 23 RSS, respectively) (Gellert, 2002). Efficient recombination occurs only when both of the RSSs are involved, termed as the 12/23 rule (Eastman et al., 1996; van Gent et al., 1995). RAGs cleave at the 5′ end of a heptamer sequence leading to the generation of the free 3′-OH group, which upon transesterification results in the generation of hairpin coding ends and blunt signal ends (Nishana and Raghavan, 2012; Schatz and Ji, 2011). Further, the coding joint is formed by non-homologous end joining following hairpin opening (Besmer et al., 1998; Malu et al., 2012; Roth, 2003; Shockett and Schatz, 1999).

In addition to its physiological function, RAGs can also cleave cryptic RSSs (cRSSs) that are abundant in the genome (Lewis et al., 1997; Roth, 2003). Various lines of evidence reveal that RAGs can cleave at non-B DNA structures (Hajj et al., 2010; Nambiar et al., 2011; Nambiar and Raghavan, 2012; Raghavan et al., 2004), resulting in cell death or chromosomal translocations and cancer, including leukemia and lymphoma. Therefore, cells must maintain stringent regulatory mechanisms for RAG expression to ensure genomic stability (Roth, 2003).

B cell development from hematopoietic stem cells is initiated in the specialized microenvironments of fetal liver and bone marrow. The early stages of B cell development are controlled

by RAG-mediated rearrangement of Ig heavy chain genes, with cells going on to become progenitor (pro-B) cells (Rodin and Thompson, 1995). Successful rearrangement of the V region to the DJ segment of the heavy chain allows entry into the precursor (pre-B) stage. Further rearrangement of the Ig light chain genes allows expression of IgM on the cell surface and differentiation into the IgM$^+$ immature B cells. These immature B cells then leave the bone marrow and migrate into the spleen to form naive, follicular, or marginal zone B cells. Activation of follicular B cells in the germinal center leads to the emergence of plasma cells and memory B cells (Pieper et al., 2013; Thomas et al., 2006). Recombinase activity of RAG is high during the initial stages of B cell development where V(D)J recombination occurs, and its expression either goes down or is transient at later stages (Schlissel, 2003).

Regulation at the transcriptional level by various transcription factors, such as PAX5, Ikaros, FOXO1, etc., is one of the mechanisms of RAG regulation (Amin and Schlissel, 2008; Brown et al., 1997; Jin et al., 2002; Kim et al., 2002; Kuo and Schlissel, 2009; Lauring and Schlissel, 1999; Lee et al., 2018; Wang et al., 2020). Although the expression of RAG1 is constant throughout the cell cycle, RAG2 is restricted only to the G1 phase (Li et al., 1996; Mitsuiki et al., 2002). Furthermore, occurrence of V(D)J recombination correlates with open chromatin, resulting in an additional layer of regulation (Schatz and Ji, 2011).

MicroRNAs (miRNAs) are 18- to 24-nt noncoding RNAs, which play a vital role in the post-transcriptional regulation of several genes by degrading or blocking the translation of respective target mRNAs (Ambros, 2004; Gebert and MacRae, 2019; Kim, 2005). miRNA expression has been studied extensively in the immune system and shown to be deregulated in cancers of immunological origin (Mansoori et al., 2013; Mi et al., 2007; Wang et al., 2012). The first miRNA reported to have a role in B cell differentiation was miR-181a, which is differentially expressed in T and B cells. Later, it was shown to play an essential role in the modulation of TCR signaling in thymocytes (Ebert et al., 2009; Li et al., 2007), suggesting that miRNAs play distinct roles in different cell lineages by affecting various sets of target genes.

The miR-29 family of miRNAs, highly expressed in the T and B cells, is required for the survival and differentiation of mature B cells (Landgraf et al., 2007; Liston et al., 2013). miR-29 null mice display no change in progenitor or immature B cell populations, suggesting that early B cell development is not affected in these mice. However, a reduction in total B cells in the spleen, owing to increased apoptosis of mature B cells, establishes the role of miR-29 in B cell maturation and proliferation (Rhinn et al., 2020). The miR-29 family consists of three members, miR-29a, miR-29b, and miR-29c. miR-29a and miR-29b-1 are encoded on human chromosome 7q32.3, and miR-29b-2 and miR-29c are located on chromosome 1q32.2 (Kwon et al., 2013). Although all three family members of miR-29 share a common 7-nt seed sequence, there are notable differences between the members (Kwon et al., 2013).

Among dozens of miRNAs that have been reported to be deregulated in cancer, the miR-29 family has been recognized to play a crucial role in altering the genetic landscape in cancer. Transcriptional profiling of miRNA expression across tumor tissues or cancer cell lines revealed that miR-29 is downregulated in most cancers, pointing to its tumor-suppressive role in cancer (Jiang et al., 2010). It exerts its anti-tumorigenic effect in various ways, which include inhibition of DNA methyltransferases (DNMTs) leading to global hypomethylation and de-repression of tumor suppressors, such as phosphatase and tensin homolog (PTEN) and WW domain-containing oxidoreductase (WWOX) (Fabbri et al., 2007; Garzon et al., 2009b); cancer cell apoptosis by downregulating anti-apoptotic proteins, such as MCL-1 and BCL-2, and upregulating pro-apoptotic proteins (Garzon et al., 2009a; Xiong et al., 2010); and cell-cycle arrest through downregulation of Cyclin E (Wang et al., 2011). Despite tremendous advancement in this field in the last few years, several key questions remain unanswered, which include the role of miRNA in the regulation of RAG expression, function, and its importance in the bias shown toward the selection of V, D, and J segments during V(D)J recombination.

In the present study, we evaluate the potential role of miRNAs in the regulation of RAG1 expression in B cells. Using various *in silico*, *ex vivo*, and *in vivo* approaches, we identified a miRNA, miR-29c, which can regulate the expression of RAG1. Overexpression of miR-29c led to the inhibition of V(D)J recombination in cells. Interestingly, miR-29c regulated RAG1 in different developmental stages of B cells in mice. The direct interaction of miR-29c to RAG1 mRNA was elucidated by 3′ UTR reporter assay and CRISPR-Cas9-mediated modification of the miR-29c binding site, which led to an upregulation of RAG1 expression at transcript and protein levels. Thus, we demonstrate the role of a miRNA in the regulation of RAG1 in lymphoid cells.

RESULTS

To investigate the role of miRNA in the regulation of RAGs, first we analyzed using miRBase the distribution and frequency of miRNAs with respect to their length. Although the length of miRNA varied from 14 to 29 nt, the majority were 21–24 nt long (Figures S1A and S1B). miRNAs harboring seed sequence that can bind to the 3′ UTR of RAG1 were short listed from TargetScan and miRDB. Considering that expression of RAGs differs in a stage-dependent manner, profiling of differentially expressed miRNAs during B cell developmental stages was examined. To do this, small RNA sequencing (RNA-seq) datasets of mouse (accession ID Sequence Read Archive [SRA]: SRP002412), comprising pro-B, pre-B, immature, and mature B cells, were analyzed. Additional datasets of human (SRA: SRP002958), comprising centrocytes, pre-GCB (germinal center B) cells, plasma, and naive and memory B cells from NCBI-SRA, were evaluated (Figures S1C–S1E). RAG expression was elevated in centrocytes and pre-GCB cells in human tonsillar tissue and low in plasma and naive B cell stages. Because miRNAs regulate gene expression by binding to the 3′ UTR of mRNAs, raw reads selected from RNA-seq datasets were mapped onto mm10 and hg19, mouse and human reference genomes, respectively, using Bowtie aligner, and mapped reads were analyzed (Figure 1A). The results suggest that although many miRNAs could be responsible for the regulation of RAG1 in various cell types and tissues, only miR-29c-3p expression inversely correlated to *RAG1* at different stages of B cell development. The results also highlight the conserved role of miR-29c-3p across humans and mice to regulate RAG1 (Figures 1B and S1G–S1I).

We obtained miRNAs targeting RAG1 and RAG2 from TargetScan, miRDB, and NCBI databases (1,173 against human

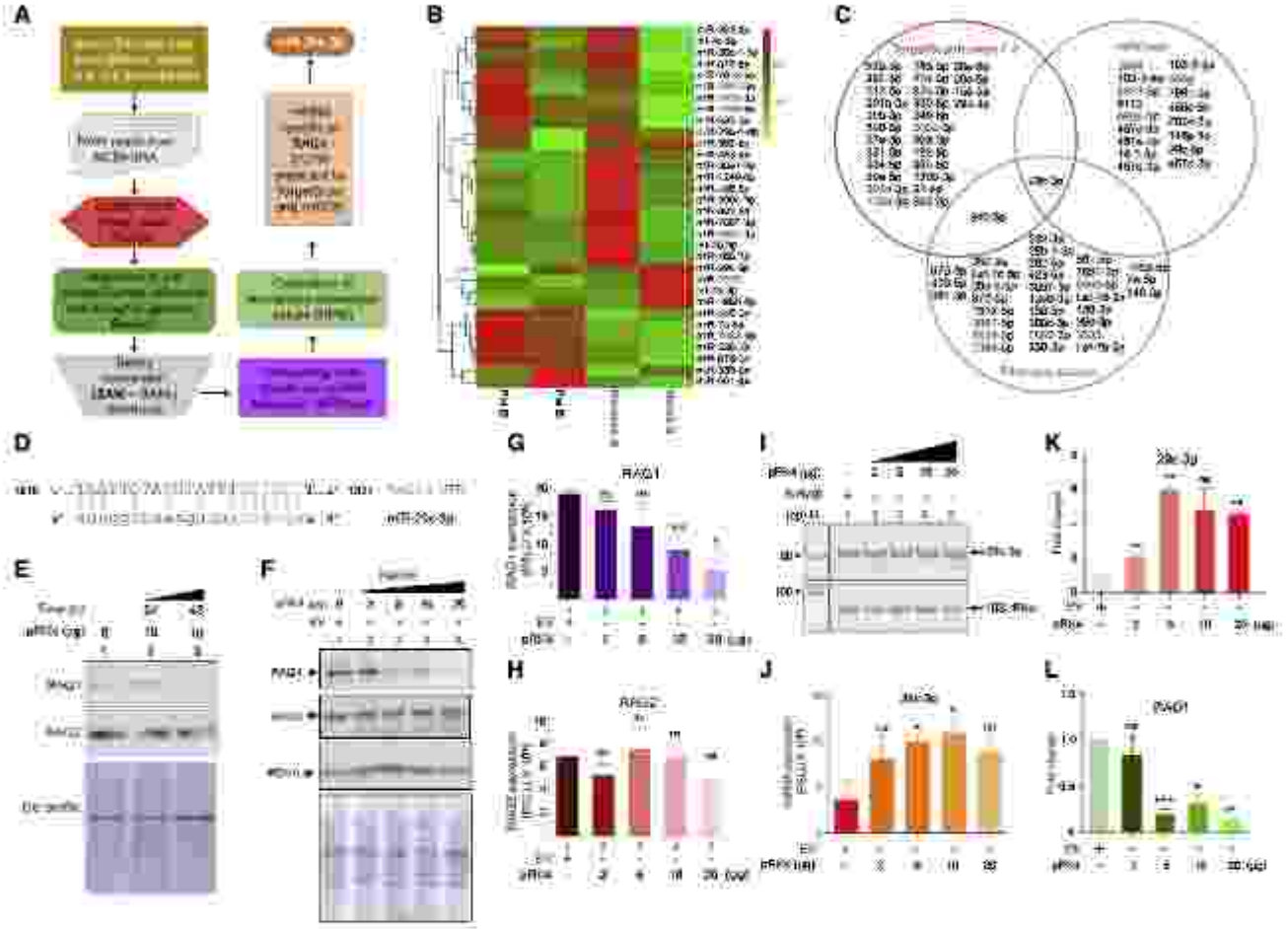

Figure 1. In silico prediction of miRNAs that can potentially target RAG1 and its impact on RAG expression following overexpression of pre-miR-29c

(A) Workflow used for identifying miRNAs predicted to bind to *RAG1 3′ UTR*.

(B) Heatmap for differentially expressed miRNAs in B cell stages based on RNA-seq datasets from NCBI public repository (accession ID SRA: SRP002412).

(C) Venn diagram showing common miRNAs when compared between databases: TargetScan human 7.2 and miRDB along with selected RNA-seq dataset (NCBI SRA).

(D) Binding sites of miR-29c-3p on *RAG1 3′ UTR*. Sequence in red represents the seed sequence of miRNA against *RAG1 3′ UTR*.

(E) Impact on expression of RAGs following overexpression of miR-29c after different time points (24, 48 h). Namalwa cells were transfected with pRK4, an episome, containing pre-miR-29c. Cells were harvested, and expression of RAG1 and RAG2 was evaluated by western blotting. The SDS-PAGE profile was used as the loading control.

(F) Evaluation of miR-29c overexpression on RAG levels. Namalwa was transfected with increasing concentrations of pRK4 (2, 5, 10, and 20 μg). Immunoblotting was performed using anti-RAG1 and -RAG2. SDS-PAGE profile and proliferating cell nuclear antigen (PCNA) were used as the loading control.

(G and H) Bar diagram showing quantification of expression levels of RAG1 (G) and RAG2 (H) following miR-29c overexpression in Namalwa ($n = 3$) after normalization with loading control, PCNA.

(I) The expression profile of miR-29c-3p at RNA level. Semiquantitative PCR was performed following transfection with increasing concentrations of pRK4. *18S rRNA* served as the loading control.

(J) Quantification of miR-29c-3p expression, following transfection of pRK4, after normalization with internal control, *18S rRNA* ($n = 4$).

(K and L) Bar graphs showing the qPCR analysis of the level of miR-29c-3p (K) and RAG1 (L) after transfection with increasing concentrations of pRK4. The values were normalized with *18S rRNA* according to the $2^{-\Delta\Delta C_T}$ method ($n = 3$).

In all panels, cells transfected with empty vector (20 μg) served as the vector control. Error bar was calculated as mean ± SEM. *$p < 0.05$, **$p < 0.005$, ***$p < 0.0001$, ns, not significant; PSLU, photo-stimulated luminescence unit.

RAG1 and 749 against mouse RAG1; 181 against human RAG2 and 116 against mouse RAG2) (Figures S1G–S1K). Of that only 18 miRNAs showed expression in all stages of tonsillar tissue (Figure S1G), and 29 miRNAs showed expression during mouse B cell development (Figures 1B, 1C, S1H, and S1I). Further, we assigned miRNA expression levels from lowest to highest (1–4). Interestingly, only one miRNA showed a negative correlation with RAG1 expression in both mouse (mmu-miR-29c-3p) and human (hsa-miR-29c-3p) samples (Figures 1B–1D and S1G–S1I). Next, we compared the miRNAs against RAG2 from

TargetScan (972) with those present in our data (279) and found that 143 miRs overlap (Figures S1J and S1K). Of those, around 15 miRNAs showed differential expression in various stages of B cell development. However, none showed a B cell stage-dependent increase in expression (Figure S1K).

Overexpression of pre-miR-29c resulted in downregulation of RAG1

To study the effect of miR-29c on the expression of RAG1, the pre-miR-29c, along with flanking sequences at both 5′ and 3′ ends, were cloned into the expression vector, pIRES2-EGFP, in physiological orientation, sequenced, and termed as pRK4 (Figures S2A and S2B). The episome (10 μg) was transfected into a pre-B cell line, Nalm6 (24 and 48 h). Interestingly, results showed a time-dependent decrease in the expression of RAG1, suggesting the inhibitory effect of miR-29c on RAG1 expression (Figure 1E). However, there was no significant effect on the expression of RAG2 (Figure 1E). Increasing concentrations of pRK4 (2, 5, 10, and 20 μg) were transfected into pre-B cell lines, Nalm6 and Reh (48 h). A concentration-dependent decrease in RAG1 expression was observed in pRK4 transfected cells compared with control (empty vector) (Figures 1F, 1G, S2C, and S2D). However, there was no significant difference in the expression levels of RAG2 (Figures 1F, 1H, S2C, and S2D). Thus, our data suggest that expression of RAG1 is significantly reduced upon overexpression of pre-miR-29c in pre-B cell lines.

Enrichment of mature miR-29c following pRK4 transfection in Nalm6 cells

The generation of mature miRNAs inside the cells was tested following transfection with pre-miR-29c construct (pRK4). Nalm6 cells were transfected with increasing concentrations of pRK4 (2, 5, 10, and 20 μg) (Figure 1I). Following RNA isolation and cDNA preparation, genomic DNA contamination in cDNA preparation was ruled out by DNase treatment and using the *HPRT* gene-specific primers to amplify RT-treated samples (Figures S2E–S2G). A consistent increase in the miR-29c-3p transcript levels with increasing concentrations of pRK4 revealed the generation of mature miRNAs inside the cells, following endogenous processing of the pre-miRNAs by the RNA-induced silencing complex (RISC) (Figures 1I and 1J). It is important to point out that the endogenous expression level of miR-29c-3p was detectable, even in the control sample (Figure 1I, lane 1), and the level was significantly enhanced upon transfection of pRK4, leading to overexpression of mature miR-29c-3p. Consistently, a significant enhancement in the expression level of miR-29c-3p was also observed when investigated following qRT-PCR (Figure 1K). A concomitant reduction in the RAG1 transcript compared with the empty vector further strengthens the hypothesis of miR-29c-mediated regulation of RAG1 (Figure 1L). Thus, we conclude that endogenous processing of pre-miR-29c into mature miRNA, miR-29c-3p, inside the cells leads to RAG1 repression in pre-B cells.

Inhibition of miR-29c-3p by anti-miR leads to elevated expression of RAG1

Chemically modified antisense oligonucleotides, termed anti-miRs, sequester mature miRNA, leading to functional inhibition of the miRNA and de-repression of its target genes. To investigate the effect of inhibitors of miR-29c-3p on RAG1 expression, we transfected Nalm6 cells with increasing concentrations of anti-miR oligomer (10, 25, 50, and 100 nM) by using Oligofectamine (Figures 2A and 2B). Cells were harvested after 48 h, and cell-free extracts were prepared. Western blotting for RAG1 showed enhanced expression of RAG1 in an anti-miR-29c-3p concentration-dependent manner (Figures 2B and 2C). No significant modulation was observed in RAG2 levels (Figures 2B and 2C), confirming the role of miR-29c-3p specifically in the regulation of RAG1.

Enrichment of 3′ UTR of RAG1 within the cells leads to enhanced expression of RAG1

We further investigated whether RAG1 expression could be enhanced on enrichment of the 3′ UTR of *RAG1* containing the miR-29c-3p binding site that would act as miRNA sponges (Figure 2D). The length of the *RAG1* 3′ UTR is ~3.3 kb. There is no homology between *RAG1* and *RAG2* 3′ UTR; thus, we did not observe any significant alteration of RAG2 on overexpression of pRK4. A 456-bp region of 3′ UTR of *RAG1* containing the miR-29c-3p binding site was cloned into the expression vector, pMIR-RECK, to generate pRK12 (Figure S2H). Nalm6 cells were transfected with increasing concentrations of pRK12 (2, 5, 10, and 20 μg). Plasmid containing random sequence served as vehicle control (20 μg). An increase in RAG1 expression was noted upon enrichment with *RAG1*-3′ UTR in Nalm6 cells (Figures 2E and 2F); however, no significant alteration in RAG2 expression was observed (Figures 2E and 2F). Thus, our results suggest that enrichment of 3′ UTR of *RAG1* within cells acts as a sponge for miR-29c-3p, leading to the enhanced expression of RAG1.

Disruption of the miRNA processing pathway alters the RAG1 expression profile

To investigate the involvement of the miRNA pathway in the regulation of RAG1 expression, we subjected the endoribonuclease, Dicer, required for the processing of pre-miRNA into functional dsRNA (Kettling et al., 2001), to short hairpin (sh)RNA)-mediated knockdown in Nalm6 cells (Figures 2G and 2H). The cells were harvested after transfection (48 h), and immunoblotting was performed to assess RAG1 levels following Dicer knockdown (Figure 2H). An increase in the RAG1 expression upon Dicer knockdown compared with cells transfected with scrambled plasmid alone establishes the role of the miRNA pathway in RAG1 regulation (Figures 2H and 2I). The Argonaute 2 (Ago2) protein, which is a part of the RISC, is essential for binding of the miRNA to its target mRNA and subsequent cleavage or translational repression of the mRNA by the RISC (Carmell et al., 2002; Hammond et al., 2001; Pillai et al., 2004) (Figure 2G). To determine the specific binding of Ago2 to RAG1 mRNA, we performed an endogenous pull down of Ago2 protein in bone marrow cells isolated from 4- to 6-weeks-old C57BL/6 mice. Expression of both miR-29c-3p and RAG1 could be detected in Ago2 immunoprecipitated (IPed) cells by RT-PCR, thus establishing the role of miR-29c-3p in regulating RAG1 expression in B cells (Figures 2J, 2K, and S2I). Consistent with this, *in silico* studies using datasets from a nonlymphoid cell line 22rv1, derived from prostate cancer,

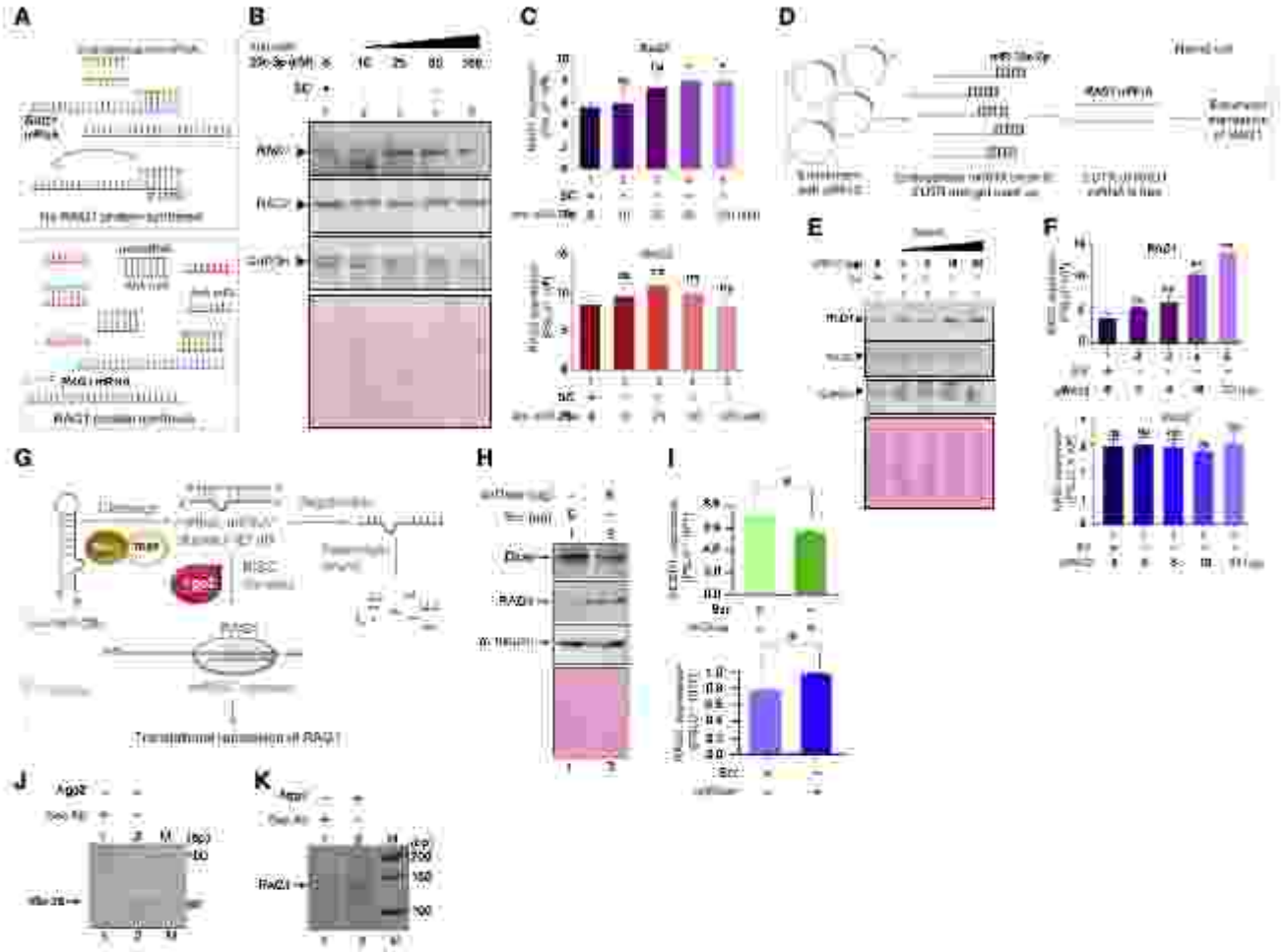

Figure 2. Evaluation of target specificity and mechanistic insights of miR-29c-3p on RAG1 expression

(A) Schematic of miRNA binding to 3′ UTR of *RAG1* and post-transcriptional gene silencing. Anti-miRs, when present, can bind to mature miRNA, leading to reduction in the pool of endogenous miRNA, resulting in RAG1 expression.

(B) Nalm6 cells were transfected with increasing concentrations of anti-miR-29c-3p (10, 25, 50, and 100 nM). Lane 1 is scrambled control (SC; 50 nM). Western blotting was performed using anti-RAG1 and anti-RAG2. Ponceau-stained blot and GAPDH served as the loading control.

(C) Bar graph showing the quantification of RAG1 and RAG2 expression after transfection with anti-miR-29c-3p ($n = 3$). A p value <0.05 was considered significant.

(D) Schematic showing enrichment of 3′ UTR of *RAG1* (which present in an episome: pRK12) that has a binding site for the seed sequence of miR-29c-3p. miR-29c-3p binding to the overexpressed mRNA possessing 3′ UTR of *RAG1* results in free endogenous RAG1 mRNA, which can get translated.

(E) Expression of RAG1 and RAG2 following transfection with increasing concentration (2, 5, 10, and 20 μg) of pRK12 in Nalm6 cells. Empty vector (EV; 20 μg) served as control. Ponceau-stained blot and GAPDH served as loading control.

(F) Bar graph showing quantification of RAG1 and RAG2 levels after transfection with pRK12 ($n = 3$). Error bar was calculated as mean ± SEM. *$p < 0.05$, **$p < 0.005$, ***$p < 0.0001$

(G) Schematic representation of the processing of pre-miRNA into mature miRNAs inside the cells. The pre-miRNA is exported by Exportin 5 from the nucleus to the cytoplasm, where it is cleaved into an imperfect dsRNA duplex by the Dicer. The guide strand of this duplex is subsequently loaded onto the RISC, containing Argonaute (AGO2) and other proteins. Binding of the seed sequence of miRNA to the miRNA recognition elements (MREs) within the 3′ UTR of *RAG1* mRNA leads to repression of its function.

(H) Immunoblotting to determine the expression of Dicer and RAG1 after shRNA-mediated knockdown of Dicer in Nalm6 cells. Scrambled (SC) plasmid (5 μg) was used as control. Ponceau-stained blot and α-tubulin served as loading control.

(I) Bar graph denotes the quantification of Dicer (upper panel) and RAG1 (lower panel) expression following knockdown of Dicer ($n = 2$). $p < 0.05$ was considered significant.

(J and K) PCR amplification of miR-29c-3p (J) and RAG1 (K) in Ago2-IPed sample in bone marrow cells isolated from 4- to 6-week-old mice. Anti-rabbit IgG was used as the secondary control. "M" denotes 50-bp ladder.

showed high high-throughput sequencing of RNA isolated by crosslinking immunoprecipitation (HITS-CLIP) signals at genomic locations of miR-29c and RAG1 3′ UTR, along with a significantly low normalized expression of RAG1, which further validates our finding (Figure S2J) (Hoecker et al., 2012).

miR-29c-3p shows target specificity toward the 3′ UTR of *RAG1*

Target specificity of miR-29c-3p was further tested using conventional 3′ UTR reporter assay (Jin et al., 2013). A 456-bp region from the 3′ UTR of *RAG1* containing a binding site for the seed sequence of miR-29c-3p was cloned into pmirGLO, downstream of luciferase gene, to generate pRK17. A mutant of *RAG1* 3′ UTR, containing the mutated binding site for seed sequence of miR-29c-3p, was also cloned to generate pRK15. Wild-type (WT) and mutant episomes were transfected into Nalm6 cells along with transfection control (β-galactosidase vector) and subjected to luciferase assay (Figure 3A). Luciferase counts were normalized with respect to β-galactosidase levels. Results showed a significant decrease in luciferase expression in WT episome relative to its mutant (Figure 3B). These results further confirm the binding of miR-29c-3p specifically to *RAG1* 3′ UTR and validate the functional downregulation of *RAG1* gene expression.

CRISPR-Cas9-mediated genome editing reveals that miR-29c recognizes the *RAG1* 3′ UTR genomic locus and modulates RAG1 expression inside the cells

To determine the direct interaction between miR-29c and *RAG1* 3′ UTR inside the cells, we used CRISPR-Cas9 to mutate the miR-29c binding site of the *RAG1* 3′ UTR at the genomic loci. Toward this, we designed two single guide RNAs (sgRNAs) around the miR-29c binding site (Figure S3A). For the first sgRNA, the construct was designed such that the PAM site was situated downstream of the miR binding site (Figure 3C). sgRNA2 was selected with the PAM site placed on the minus strand upstream of the miR binding site. An HDR (homology-directed repair) construct was also generated where the miR-29c target sequence TGGTGCT was mutated to TAGCGAT using site-directed mutagenesis, along with mutation of the PAM site from GGG to GTG (Figure 3C). The pre-B cell line, Nalm6, lacking NHEJ was transfected with sgRNA1, sgRNA2, or both, along with different combinations of HDR construct (Figure S3D). The puromycin-resistant clones were selected (Figure S3E), and genomic DNA from the putative mutant clones and WT cells was isolated, followed by a competition-based PCR strategy to check the mutation at the *RAG1* 3′ UTR (Figure S3B). Three primers were designed, of which one was forward (F1) and two reverse (R1 and R2) (Hariparsa and Raxman, 2017). The F1 and R1 primers gave an amplicon of 421 bp, and F1 and R2 generated an amplicon of 211 bp. The R2 3′ region was complementary to the miR-29c binding site; thus, a mutation at this site would lead R2 unable to pair to the DNA, and therefore, no extension from R2 would occur in the mutant (Figure S3B). When all three primers were used in a single reaction, the 421-bp amplicon would be observed for the clones, whereas the WT would have higher-intensity amplification for the shorter (211-bp) amplicon. We observed that out of the five clones tested, three clones showed a faint or no band for the shorter amplicon, but the larger fragment was amplified (Figure S3C). Further, a 421-bp fragment from clone B5, termed as N6-29c-B5, was sequenced and confirmed the precise mutation at the 3′ UTR of *RAG1*, along with the PAM site mutation (Figures 3D and S3F).

To evaluate the expression of RAG1 in N6-29c-B5 at the transcript level, we performed semiquantitative and qRT-PCR. There was a significant increase in the RAG1 transcript compared to WT cells (Figures 3E–3G). A distinct increase in RAG1 expression was observed at the protein level in N6-29c-B5, when analyzed using western blotting (Figures 3H and 3I). These results suggest that knockout (KO) of the miR-29c binding site directly affected RAG1 expression within the cells, confirming involvement of miR-29c in *RAG1* regulation. This is consistent with studies showing mutation of the *RAG1* 3′ UTR miR-29c binding site increased the expression of luciferase compared with the WT *RAG1* 3′ UTR miR binding site.

Overexpression of miR-29c-3p inhibits V(D)J recombination within cells

To investigate the effect of miR-29c on V(D)J recombination, we performed multiple combinations of extrachromosomal V(D)J recombination assays in the Nalm6 cell line (Figure 4A). In this assay, cells were transfected with the episomes, pGG51 or pGG49, which reconstitute joining due to coding joint and signal joint, respectively (Figure 4A). During V(D)J recombination, 12RSS and 23RSS sequences are recognized and cleaved by RAG1. Because the signal sequences are positioned in such a way that recombination will lead to the removal of intervening transcription terminator, the recombinants acquire resistance to chloramphenicol, post-V(D)J recombination (Figure 4A). We transfected Nalm6 cells with the constructs pGG49 or pGG51, along with pRK4 (10 μg) or pRK12 (10 μg), followed by harvesting of the episomal DNA and transformation into *E. coli* DH10β. Recombinants were selected on Amp^r+Chl^r (CA) Luria Bertani (LB) agar plates, and total plasmid isolated was analyzed on Amp^r (A) plates. The recombination efficiency was calculated as CA/A × 100, reflecting the fraction of recovered substrates that underwent V(D)J recombination.

Upon co-transfection of pGG51 with miR-29c overexpression plasmid pRK4, we observed a significant reduction (1.7-fold) in the recombination efficiency (Figures 4B and S4A). Similarly, when we used pGG49 construct along with pRK4, V(D)J recombination efficiency was reduced by 2.3-fold, suggesting miR-29c affected RAG-mediated recombination (Figures 4D and S4C). Recombination was confirmed by DNA sequencing for coding and signal joint formation (Figures 4F and 4G). Further, we hypothesized that if miRNA is involved in RAG1 regulation, then overexpression of *RAG1* 3′ UTR will lead to sequestration of endogenous miRNAs regulating RAG1, causing increased RAG1 expression and, in turn, V(D)J recombination. Toward this end, we transfected V(D)J episomal constructs along with pRK12 (harboring a portion of 3′ UTR of *RAG1* containing the seed sequence of miR-29c) and observed a significant increase in recombination efficiency (2- to 2.3-fold) with respect to both coding and signal joint formation (Figures 4C, 4E, S4B, and S4D). Thus, miR-29c can modulate the physiological function of RAG1 inside cells by altering the efficiency of V(D)J recombination (Figure 4H).

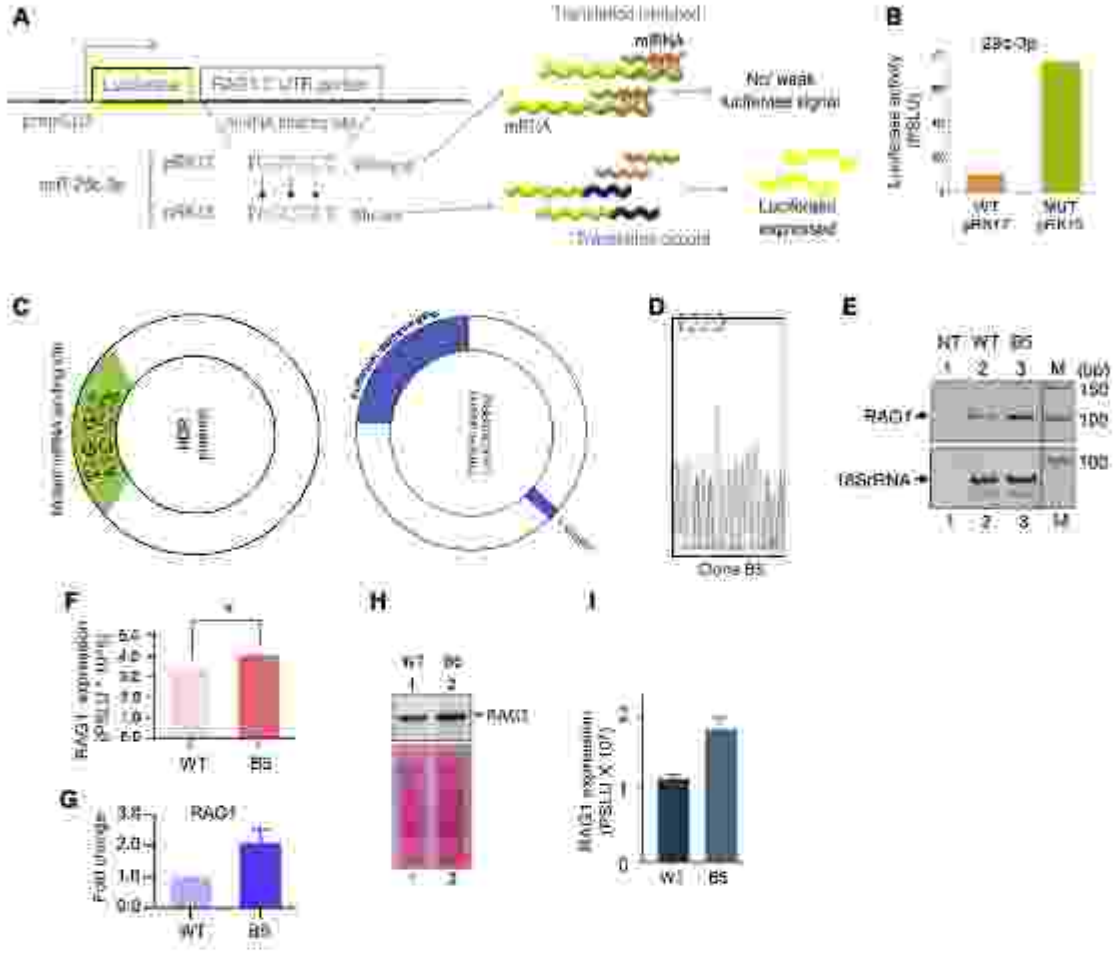

Figure 3. Evaluation of target specificity within cells using luciferase assay and CRISPR-Cas9-mediated modification of miR-29c binding site at RAG1 3′ UTR at genomic locus

(A) Schematic representation of plasmid containing 3′ UTR of *RAG1* or its mutant cloned downstream to luciferase gene. Upon transfection, a chimeric mRNA is synthesized under the influence of upstream promoter. In the presence of wild-type (WT) binding site for miRNA in *RAG1* 3′ UTR will be occupied by miRNA to bring about translational repression of luciferase expression, which can be measured by a luminometer. When mutant 3′ UTR of *RAG1* is present, luciferase expression remains uninhibited, resulting in intense signals. Yellow-colored box represents the luciferase gene, green represents the WT 3′ UTR of *RAG1*, and purple represents the mutant.

(B) Bar graph showing the luciferase activity in Namalwa cells after transfection with pRK17 (WT) and pRK15 (mutant).

(C) To study RAG1 expression following CRISPR-Cas9-mediated genome editing in the miR-29c binding site, we used the vector LentiCRISPRv2 as the backbone for the construction of sgRNAs targeting the miR-29c binding site at the *RAG1* 3′ UTR (pMS51, 52). An HDR construct was generated wherein the *RAG1* 3′ UTR containing the mutated miR-29c binding site was cloned (pMS53).

(D) Sequencing results for the CRISPR-Cas9-generated miR-29c clone B5 shows the expected mutation in the miR-29c binding site of RAG1 3′ UTR.

(E) Expression analysis of RAG1 using semiquantitative PCR of WT and mutated clone B5. *18S rRNA* was used as the internal control. "M" denotes 50-bp ladder.

(F) Bar graph showing the change in the expression of RAG1 transcript as measured by semiquantitative PCR ($n = 3$).

(G) Bar graph showing the fold change in the expression of RAG1 transcript through qRT-PCR. The values were normalized with *18S rRNA* according to the $2^{-\Delta\Delta Ct}$ method ($n = 3$).

(H and I) Immunoblot analysis of RAG1 expression in WT and the mutant clone, B5. Ponceau-stained blot served as the loading control (H). Bar diagram depicts the level of RAG1 in WT and mutant clone (I).

(F, G, and I) Error bar was calculated as mean ± SEM. $^{*}p < 0.05$, $^{**}p < 0.005$, $^{***}p < 0.0001$ in all cases.

miR-29c-3p exhibits a stage-specific expression that is inversely proportional to RAG1 during B cell development in mice

To study the expression profile of miR-29c-3p during B cell development in mice, we sorted different stages of B cells using B cell stage-specific markers, $CD45R^{+}/CD43^{+}$ (pro-B cells), $CD45R^{+}/CD25^{+}$ (pre-B cells), $CD45R^{+}/IgM^{+}$ (immature B cells), and $CD45R^{+}/IgM^{+}/IgD^{+}$ (mature B cells) (Figures 5A and 5B). PCR amplification of miR-29c-3p and RAG1 was performed to compare their expression profiles across different stages of B cell development. Results showed significantly lower levels of miR-29c-3p in pro- and pre-B cells, where RAG1 expression

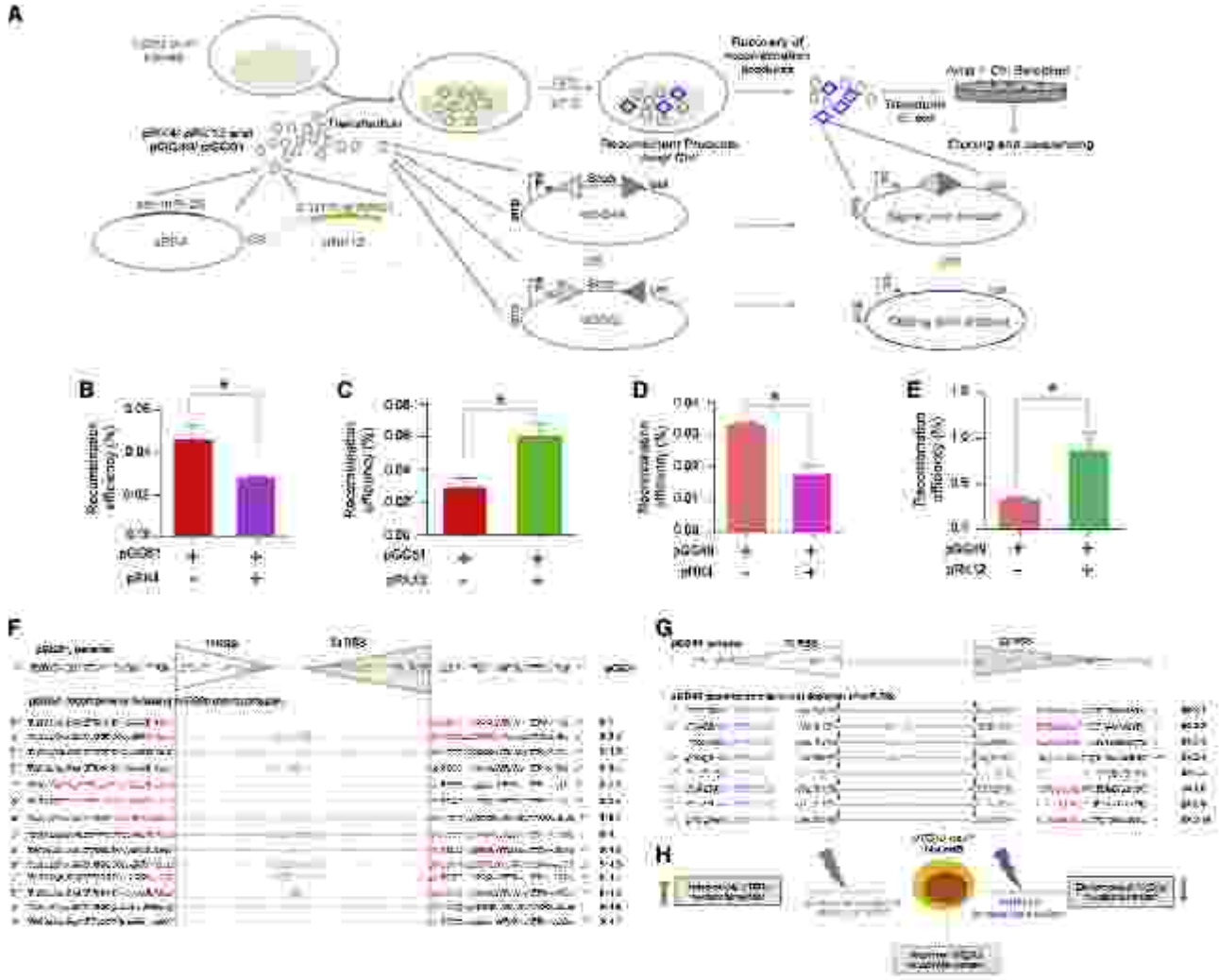

Figure 4. Assessment of V(D)J recombination potential of pro-B cells upon co-transfection of pre-miR-29c or *RAG1* 3′ UTR

(A) Outline of the extrachromosomal V(D)J recombinase assay. The diagram depicts the transfection of episomes into the pre-B cell line, Nalm6, active for V(D)J recombination. After 72 h, the minichromosomes were harvested, then transformed into *E. coli* for detection of recombinants on ampicillin (*A*) and chloramphenicol (CA) LB agar plates. The recombination is depicted between a consensus 12 signal (open triangles) and 23 signal (dark green triangles) leading to either coding joint formation (pGG51) or signal joint formation (pGG49). "*cat*" denotes the chloramphenicol acetyltransferase gene, and "*stop*" denotes the prokaryotic transcription terminator. The *E. coli lac* promoter is denoted as P_{lac}. The episome, pGG49 or pGG51 (5 μg), was co-transfected with either pRK4 (10 μg) or pRK12 (10 μg), and the recombination efficiency was determined by the formula: (CA/A) × 100.

(B and C) The bar graphs indicate the change in the recombination efficiency in the presence of either pRK4 ($n = 3$) (B) or pRK12 ($n = 3$) (C) when transfected with pGG51.

(D and E) The graphs indicate the change in the recombination frequency in the presence of either pRK4 ($n = 4$) (D) or pRK12 ($n = 4$) (E) when pGG49 was used for investigation.

(F) Sequence of the parental plasmid, pGG51 (upper panel). The open triangle represents 12 RSS, while the closed triangle represents 23 RSS. Colored sequences in the RSS represent the heptamer and the nonamer. Sequencing results of the recombinant plasmids showing the formation of a coding joint between 12 and 23 RSSs after RAG-mediated recombination (lower panel). Sequences in red represent the deletions, and sequences in green represent the insertions.

(G) Sequence of the parental plasmid, pGG49 (upper panel). Sequencing results of the recombinant plasmids showing the formation of a signal joint after RAG-mediated recombination (lower panel).

(H) Schematic representation summarizing the effect of overexpression of either pre-miR-29c (blue arrow) or *RAG1* 3′ UTR construct (green arrow) on V(D)J recombination.

was high (Figures 5C–5E). Interestingly, expression of miR-29c-3p was ~4-fold higher in both immature and mature B cells, where RAG1 expression was less compared with pro- and pre-B cells (Figures 5C–5E). The band corresponding to miR-29c-3p was PCR amplified from different stages of B cells, gel purified, and cloned, and identity was confirmed by sequencing (Figure 5F). A 72% homology between mouse and human RAG1 3′ UTR and the presence of miR-29c binding site on both the UTRs explains the miR-29c-mediated regulation of RAG1 expression conserved across both species (Figure S1F).

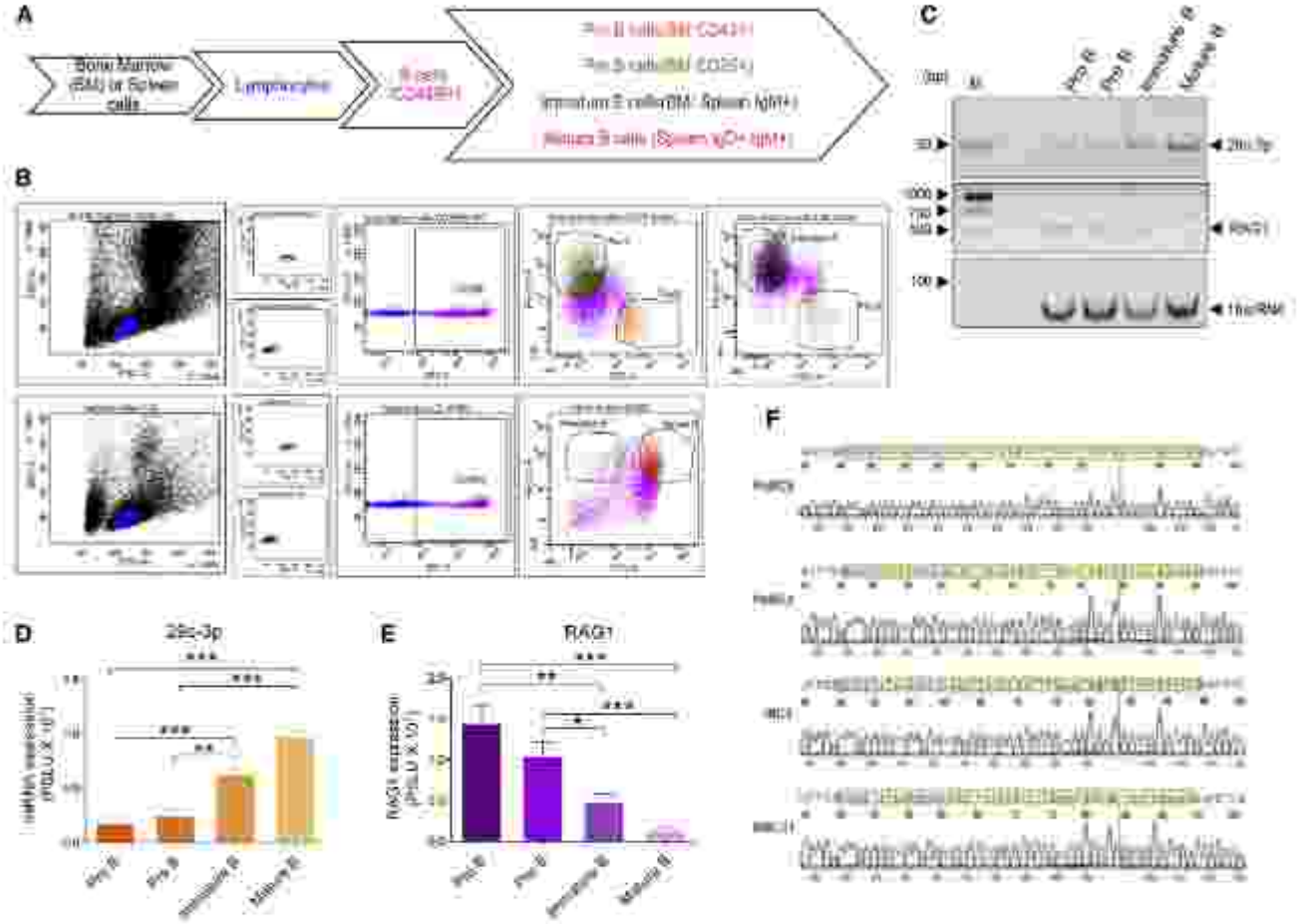

Figure 5. Evaluation of stage-specific expression of miR-29c-3p and RAG1 during B cell development

(A) Flow diagram explaining the isolation of different stages of B cell populations using fluorescence-activated cell sorting (FACS). Lymphocytes were gated from murine bone marrow and spleen, following which all CD45R+ B cells were gated, from which pro-B cells (CD43+), pre-B cells (CD25+), immature B cells (IgM+), and mature splenic B cells (IgM+ IgD+) were sorted.

(B) Representative FACS plots for isolation of murine B cells from four B cell developmental stages: pro-B, pre-B, immature B cells from bone marrow (upper panel), and mature B cells from spleen (lower panel).

(C) Semiquantitative RT-PCR showing the endogenous expression level of miR-29c-3p and Rag1 in isolated murine B cells by using specific primers. 18S rRNA was used for normalization.

(D and E) Bar diagrams showing the quantification of PCR amplification of miR-29c-3p (D) (n = 3) and RAG1 (E) (n = 3) in different stages of B cells. For each sorting experiment, bone marrow and spleen cells were pooled from three mice, respectively. Error bar was calculated as mean ± SEM. *p < 0.05, **p < 0.005, ***p < 0.0001.

(F) Chromatograms for miR-29c-3p sequence from pro-B (Clone No. PoBC5), pre-B (Clone No. PeBC2), immature B (Clone No. IBC4), and mature B cells (Clone No. MBC1). miR-29c-3p band was gel purified after PCR amplification from different stages of B cells, cloned in TA vector, and sequenced. The sequence of miR-29c-3p is boxed and indicated using green color.

Knockout of miR-29c in mice leads to reduction in mature B lymphocyte population

Several lines of experimentation in cell line models successfully established the role of miR-29c in regulating RAG1 expression. In order to evaluate the impact of miR-29c during B cell development, we analyzed the total lymphocyte population from lymph node and spleen of miR-29c$^{-/-}$ mice. Previously the generation of miR-29c$^{-/-}$ mice was reported using Cre-mediated deletion of the miR-b2/c locus (Dooley et al., 2016). The miR-29c KO mice were reported to be born at typical ratios and did not present any histological abnormalities (Dooley et al., 2016). We analyzed the total number of B220^{+} and CD19^{+} lymphocytes from lymph node and spleen of WT, heterozygous (HET), and miR-29c$^{-/-}$ (KO) mice (Figures 6A–6D). The percentages of mature B cells were plotted for WT, HET, and KO animals, and a consistent decrease in the total percent of B220^{+} and CD19^{+} B cells in the lymph node of most of the miR-29c$^{-/-}$ KO animals, compared with HET and WT animals, was observed (Figures 6A and 6B). The total number of CD19^{+} B cells was lower in the spleen of KO animals than WT animals (Figure 6D). However, such a difference was not evident when B220^{+} cells were analyzed from spleen (Figure 6C).

Based on the above results, we hypothesize that the reduction in total number of mature B cells could be due to increased

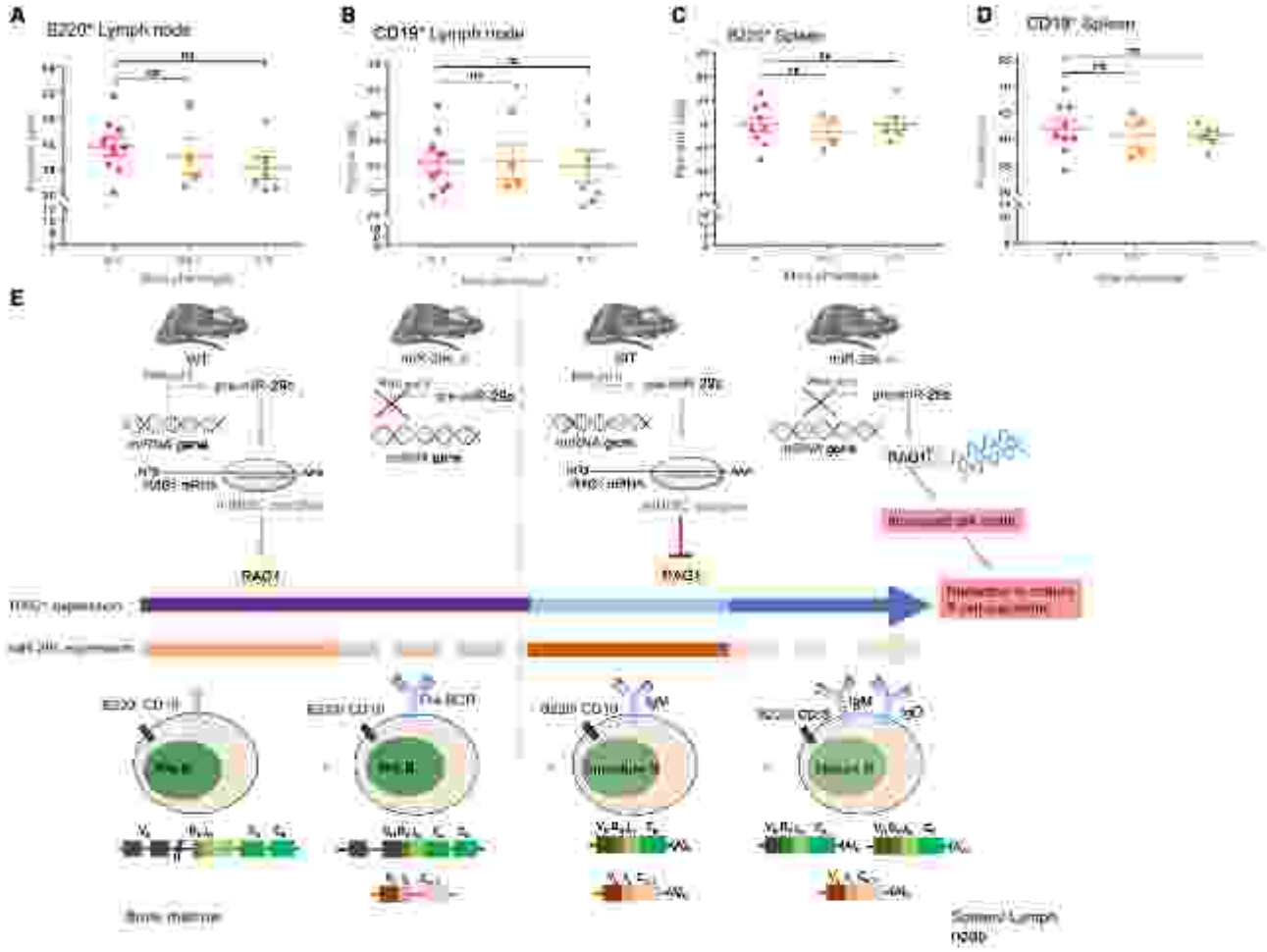

Figure 6. Impact of knockout of miR-29c on B cell development in miR-29c$^{-/-}$ mice and schematic showing mechanism of miRNA-mediated regulation of RAG1

(A–D) Analysis of lymphocytes from lymph node and spleen of miR-29c$^{-/-}$ mice. Scatterplots indicating the total lymphocyte population in the WT, HET (heterozygous), and miR-29c$^{-/-}$ (KO) mice using pan B cell markers, B220 and CD19. The percentage of lymphocytes was analyzed using FACS for lymph nodes (A and B) and spleen (C and D). Error bar was calculated as mean ± SEM. *$p < 0.05$, **$p < 0.005$, ***$p < 0.0001$.

(E) Schematic representation of miRNA-mediated regulation of RAG1. During B cell development, progenitor B cells in bone marrow undergo a sequential immunoglobulin gene rearrangement and subsequently mature in secondary lymphoid organs. Pro-B cells initiate rearrangement at Ig heavy chain locus leading to DH-to-JH joining followed by VH-to-DJH joining. At the pre-B cell stage, heavy chain assembles with surrogate light chain (SLC) to form the pre-B cell receptor (pre-BCR). The SLC is then replaced by a rearranged light chain to form IgM on immature B cells. Immature B cells then migrate from the bone marrow into the spleen as transitional B cells and develop as mature B cells expressing IgD. In the early developmental stages of B cells in WT mice, namely, pro-B and pre-B cells, miR-29c-3p expression is low, while RAG1 expression is high, and hence V(D)J recombination is active. In later stages of B cell development, i.e., immature B cells and mature B cells, miR-29c-3p expression is high, which gets incorporated in RISC and targets the 3′ UTR of RAG1 mRNA, leading to its translational inhibition.

DNA breaks generated following upregulation of RAG1 in miR-29c KO mice. Considering that miR-29c expression is low in pro- and pre-B cells, even in WT mice, further KO of miR-29c may not have an impact with respect to the early developmental stages of B cells. Thus, we believe that because RAG1 expression is tightly controlled by different regulatory elements at the transcriptional and translational level, miRNA-mediated post-transcriptional regulation represents an additional layer of regulation, the disruption of which might not drastically alter the RAG1 expression *in vivo* or mouse physiology as a whole (Figure 6E).

To investigate the endogenous levels of mature miR-29c-3p in different mouse tissues, we prepared and used cDNA to compare endogenous miRNA levels based on *18S rRNA* equalization (Figure S5A). RT-PCR revealed that although robust expression of miR-29c-3p was seen in the brain, heart, kidney, and lungs, its expression was minimal in the thymus and spleen (Figures S5A and S5B). Further, PCR products from liver and thymus tissues for miR-29c-3p were cloned, and their identity was confirmed by sequencing (Figures S5C and S5D). Thus, our results revealed that mature miR-29c-3p is generated endogenously at different levels in mouse tissues.

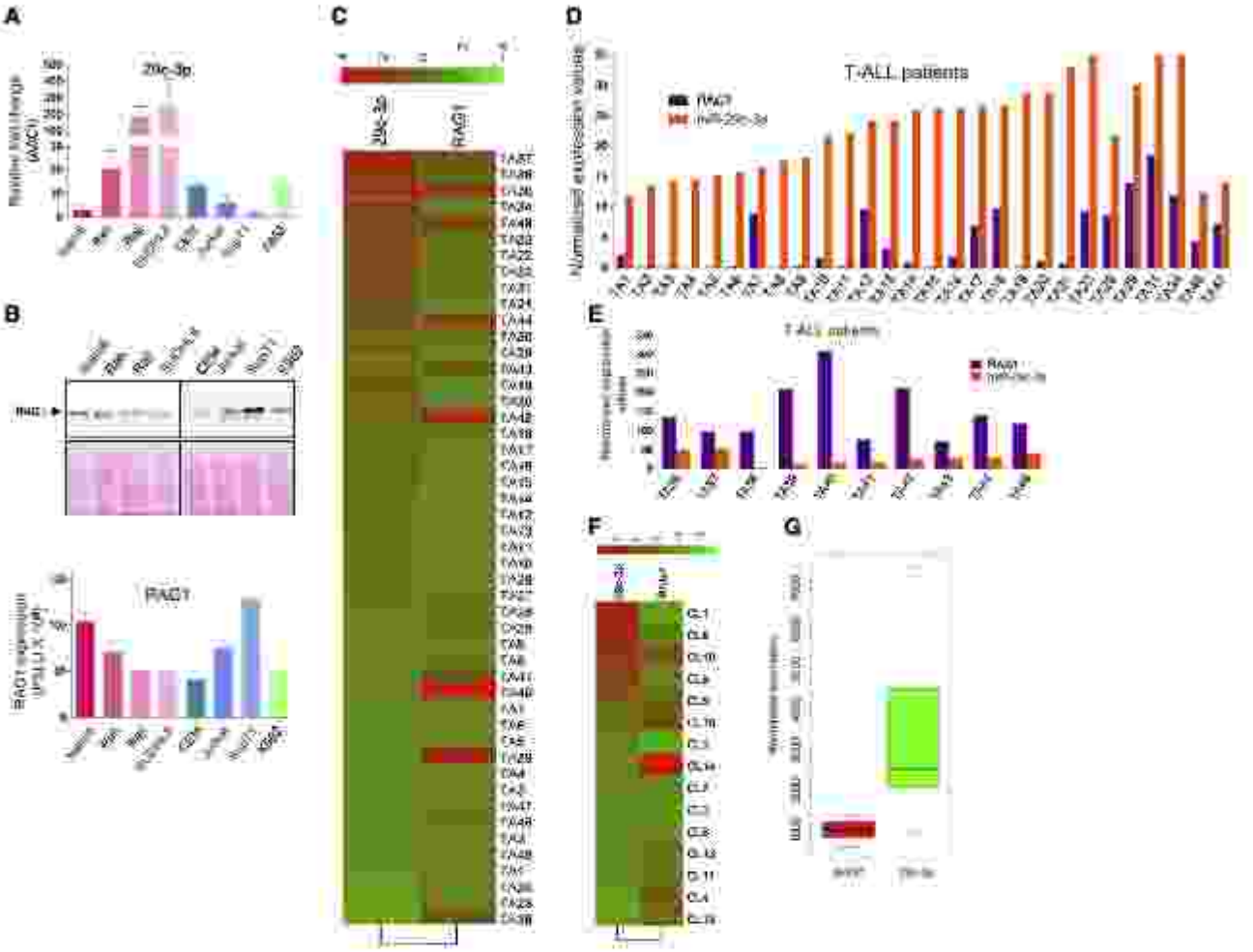

Figure 7. Evaluation of endogenous expression of miR-29c-3p and *RAG1* in different leukemia patients and cell lines

(A) Bar graph showing the fold change using $2^{-\Delta\Delta Ct}$ method of the expression of miR-29c-3p in different leukemia (Nalm6, Reh, CEM, Jurkat, SupT1, and K562) and lymphoma (Raji, SUDHL8) cell lines using qRT-PCR. *18S rRNA* was used as the internal control. Relative fold change of miR-29c-3p expression in different cell lines was calculated with respect to Nalm6 (n = 3). Error bar represents mean ± SEM.

(B) Western blotting showing expression of RAG1 in different lymphoid cell lines (upper panel). Bar graph showing the quantification of RAG1 (lower panel) in different cell lines after normalization with Ponceau-stained blot (n = 3).

(C) Heatmap showing expression profile of miR-29c-3p and *RAG1* in different T-cell acute lymphoblastic leukemia (T-ALL) patients (n = 48).

(D and E) Bar diagram showing comparative expression profiles of RAG1 and miR-29c-3p in T-ALL patients.

(F) Heatmap showing expression profile of miR-29c-3p and *RAG1* in different chronic lymphocytic leukemia (CLL) patients (n = 15).

(G) Boxplot showing comparative expression profiles of RAG1 and miR-29c-3p in CLL patients.

Endogenous expression of miR-29c-3p differs among lymphoid cell lines and is inversely correlated to RAG1 levels

Endogenous levels of mature miR-29c-3p in various lymphoma and leukemia cell lines (Nalm6, Reh, Raji, SUDHL8, CEM, Jurkat, SupT1, and K562) were determined using semiquantitative (Figure S8A) and qRT-PCR (Figure 7A). Results revealed an inverse correlation between miR-29c and RAG1 expression at transcript and protein levels (Figures 7A, 7B, and S8A). Pre-B leukemic cell lines, Nalm6 and Reh, exhibited a low level of miR-29c-3p and a high level of RAG1 protein (Figures 7A and 7B). In contrast, cell lines derived from mature B cell lymphoma (Raji and SUDHL8) exhibited elevated expression of miR-29c-3p and reduced RAG1 expression (Figures 7A and 7B). Overall, our results revealed an inverse correlation between the expression of miR-29c and RAG1 expression in most of the cell lines tested (Figures 7A and 7B).

We also analyzed miRNA-seq data derived from GCB cells, memory B cells, naive B cells, and plasma cells from human tonsillar tissue with that of data derived from cancer cell lines, such as Burkitt's lymphoma, diffuse large B-cell lymphoma (DLBCL), mantle cell lymphoma (MCL), chronic lymphocytic leukemia (CLL), and acute lymphoblastic leukemia (ALL) from lymphoid organs (SRA: SRP000729) (Figures S8B and S8C). Results showed that the level of miR-29c-3p was high in all mature B cells analyzed from normal human samples, leading to low

levels of RAG1, unlike tumor cell lines, except in the DLBCL cell line (Figures S6B and S6C). This further suggests that miR-29c-3p is negatively correlated with RAG1 in human cell lines analyzed.

RAG1 expression is inversely correlated to miR-29c-3p in T cell leukemia and CLL patients

To investigate the expression of miR-29c-3p in leukemia patients, we considered two RNA-seq datasets derived from 48 T-ALL and 15 CLL patients. The dataset, GEO: GSE66186, included 15 CLL samples (small RNA-seq and mRNA-seq), while GEO: GSE89978 included 48 T-ALL small RNA-seq samples, and GEO: GSE110637 had total RNA-seq of the samples from the GEO database (Figures S6D and S6E). Results revealed that ~79% of T-ALL patients showed an inverse correlation between miR-29c-3p and RAG1 expression (Figures 7C, S6D, and S6E). Interestingly, among these, ~58% of patients exhibited high miR-29c-3p levels (RPM [number of reads mapped per transcript/(total number of mapped reads/10^6)] values of 11–39) and low RAG1 expression (RPKM [read count/(transcript length/1,000) × (total number of reads mapped/10^6)] values ranging from 0.1 to 9) (Figures 7C and 7D), while ~20% of patients showed high *RAG1* and low miR-29c-3p expression (Figures 7C and 7E). It is important to note that ~20% of the T-ALL patients exhibited comparable levels of miR-29c-3p and RAG1 (Figures 7C and S6F). We observed that ~67% of CLL patients showed an inverse correlation with respect to expression of miR-29c-3p and RAG1 (Figures 7F, 7G, S6D, and S6E). In 53% of the CLL patients, miR-29c-3p was highly expressed (ranging from 912 to 7,507 RPKM), while RAG1 levels were low (ranging from 594 to 2,249 RPM) (Figures 7F, 7G, S6D, and S6E). These results suggest that miR-29c-3p can regulate the expression of RAG1 in leukemia patients, which might have implications in oncogenesis and tumor progression.

DISCUSSION

V(D)J recombination is a highly orchestrated process that is spatially and temporally regulated at different levels, starting from DNA sequences to chromatin structure and nuclear organization (Johnson et al., 2012). Regulation of RAG expression is one of the crucial ways of restricting V(D)J recombination. First, RAG expression is primarily restricted to lymphoid cells allowing V(D)J rearrangement to occur specifically in lymphocytes. Second, RAG2 is stable only in the G0/G1 phase of the cell cycle (Lee and Desiderio, 1999; Li et al., 1996). Lastly, V(D)J recombination occurs in the initial stages of B cell development (pro- and pre-B) during the rearrangement of the heavy and light chain, when RAG expression is high (Schlissel, 2003). The elevated expression of RAGs in early B cell stages is controlled by various transcription factors (FOXO1, BCL11A, etc.) and cis-acting enhancer elements (Erag, Ep, and Ed) (Amin and Schlissel, 2008; Chen et al., 2011; Coffre et al., 2016; Hsu et al., 2003; Lee et al., 2016).

In this study, we describe an additional mechanism of RAG1 regulation by miRNAs. Using various bioinformatics and biochemical approaches, we find that miR-29c can bind to the 3′ UTR of *RAG1*. Overexpression of miR-29c resulted in downregulation of RAG1 in pre-B cells, although there was no or minimal effect on the expression of RAG2. Specific binding of miRNA to its target mRNA was confirmed by luciferase assay and CRISPR-Cas9-mediated modification of the miR-29c binding site at the 3′ UTR of *RAG1*. Enrichment of 3′ UTR of *RAG1* within human B cells resulted in the upregulation of RAG1 because it acted as a sponge for miR-29c-3p. Further, transfection with anti-miR-29c-3p resulted in the upregulation of RAG1, confirming the role of miR-29c in *RAG1* regulation. Using extrachromosomal V(D)J recombination assay system, we observed that overexpression of miR-29c or the 3′ UTR of *RAG1* altered the recombination efficiency in a miRNA-dependent manner.

Role of miR-29c during B cell development

Various studies have reported that miRNAs regulate different stages of B cell development, ranging from hematopoietic progenitor cells in bone marrow to differentiated mature B cells in the spleen. Using Dicer-deficient mice, it was reported that miRNAs are crucial for B cell differentiation, particularly during the pro- to pre-B cell transition (Koralov et al., 2008). In the current work, *in vivo* studies in mice revealed an inverse correlation between RAG1 and miR-29c-3p in different developmental stages of B cells. These results are consistent with *in silico* studies using RNA-seq data derived from developmental stages of B cells. Consistently, we observed that level of miR-29c-3p was inversely correlated with RAG1 in B and T cell lines. Thus, our results demonstrate that miR-29c-3p can regulate RAG1 in both mouse and human B cells, implicating a direct role on the immune system.

Further enhanced level of miR-29c in immature and mature B lymphocytes results in the inhibition of RAG1. This stringent regulation of RAG1 expression may be crucial for the maintenance of genomic stability in mammals. Our study shows a decrease in the mature B lymphocyte population in lymph node and spleen of miR-29c$^{-/-}$ mice. We hypothesize that the increased RAG1 expression owing to KO of miR-29c leads to DNA breaks and damage in these cells. RAGs have been shown to cleave non-B DNA structures formed in the genome, leading to chromosomal translocations (e.g., t(11;14), t(10;14), t(14;18)) (Raghavan et al., 2001, 2004, 2005). This cleavage of non-V(D)J recombination signal in fragile regions of the genome can increase DNA breaks, cell death, and damage and ultimately leads to the reduction of mature B cells, as observed in our study. Further, mice constitutively expressing RAG genes die between 3 and 4 weeks of age and show severe lymphopenia, a phenotype reminiscent of mice defective in double-strand break repair pathway (Barreto et al., 2001). Because the miR-29c$^{-/-}$ mice show marginal survival defect and no histopathological abnormalities hampering the immunity of the mice (Dooley et al., 2010), we speculate that there would be only a minor decrease in progenitor cell population, if any. Furthermore, RAG1 expression is tightly regulated at transcriptional and translational levels, and miRNA-mediated post-transcriptional regulation represents an additional layer of regulation. However, further studies are required to evaluate the effect of miR-29c KO on progenitor cell population and immunity of an organism. Interestingly, a recent study showed that ablation of miR-29 in mouse models resulted in loss of mature cells, but not progenitor B cells (Primo et al., 2020). The authors suggested dampening of the

phosphatidylinositol 3-kinase (PI3K) signaling and subsequent increase in PTEN expression as the factors responsible for reduced survival and terminal differentiation of mature B cells (Haas et al., 2019).

miR-29c as a biomarker and potential target to treat leukemia and lymphoma

miRNAs are often expressed aberrantly in B cell leukemia and lymphoma. Therefore, several studies infer the use of miRNAs as a predictive biomarker for detection of B cell malignancies and in the development of new therapeutic strategies (Fernández-Mercado et al., 2015; Solé et al., 2018; Wang et al., 2016). We observed an inverse correlation of miR-29c with RAG1 in various B cell cancer cell lines, such as Nalm6, Reh, and Raji, suggesting their role in B cell lymphomagenesis. Consistent with this, miR-29 is deregulated in many B cell cancers (Pekarsky et al., 2006; Solé et al., 2017; Zhao et al., 2010; Zhang et al., 2014). Because the RAG complex plays a significant role in inducing DNA breaks and subsequent chromosomal translocations (Kumar and Raghavan, 2011), the observed downregulation of miR-29, and thus upregulation of RAGs in leukemia and lymphoma, could facilitate oncogenesis and progression of cancer.

Based on the expression of miR-29c-3p and RAG1, we classified T-ALL patients into three groups. The majority of patients showed high expression of miR-29c-3p and low levels of RAG1, followed by those who showed increased expression of RAG1 and low levels of miR-29c-3p. Patients who did not show any correlation formed the third group. Such patterns can have an implication in the classification of patients in different stages of T-ALL, although this aspect needs to be investigated further. Interestingly, we observed that even T-ALL cell lines showed an expression profile that matched with patient data. Further, the majority of CLL patients exhibited high levels of miR-29c-3p and low levels of RAG1. Because most of the T-ALL and CLL patients have high expression of miR-29c-3p, it could serve as a biomarker for the early detection of leukemia, which requires further studies.

Considering that miR-29 can regulate RAG1 and the latter is upregulated in many lymphoma and leukemia cases, overexpressing miR-29 or using miRNA mimics could be a therapeutic option in such cancers. On a similar line, we observed that overexpression of miR-29c led to downregulation of RAG1 and thus V(D)J recombination. From a therapeutic point of view, miRNA-based treatments involve either miRNA inhibition therapy using antisense oligonucleotide or miRNA sponges, or miRNA restoration therapy using miRNA mimics (Li et al., 2017; Shah et al., 2016). Thus, we hypothesize that because miR-29c-3p is associated with many B cell malignancies, it could be developed as a potential therapeutic candidate for B cell malignancies in the clinic. It would also be interesting to decipher the role of other members of the miR-29 family, miR-29a and miR-29b1/b2, that harbor the seed sequence for RAG1 binding in RAG1 regulation.

Thus, miRNA-mediated RAG1 regulation is an additional mechanism that restricts V(D)J recombination in a B cell stage-specific manner during lymphocyte development and could function synergistically with other regulatory elements.

STAR★METHODS

Detailed methods are provided in the online version of this paper and include the following:

- KEY RESOURCES TABLE
- RESOURCE AVAILABILITY
  - Lead contact
  - Materials availability
  - Data and code availability
- EXPERIMENTAL MODEL AND SUBJECT DETAILS
  - Animals
  - Cell lines
- METHOD DETAILS
  - Enzymes, chemicals and reagents
  - Plasmids
  - Datasets for miRNA studies
  - Method used to compute transcript expression
  - T-ALL and CLL patients' datasets used to study miRNA and RAG1 expression
  - RNA isolation and preparation of cDNA
  - Semiquantitative and quantitative PCR to analyze the microRNA expression profile
  - Cloning and sequencing of miRNAs
  - Pre-miRNA cloning
  - Quantification of miRNA expression
  - miRNA-mediated regulation of RAG1 expression at different time points
  - Immunoblotting
  - Cloning of 3′ UTR of RAG1 containing the seed sequence of miR-29c-3p
  - Site-directed mutagenesis
  - Luciferase reporter assay
  - Transfection studies with anti-miR to evaluate the effect of the miRNA on RAG expression
  - CRISPR-Cas9 mediated genome editing of miR-29c binding site in RAG1 3′UTR
  - *In vivo* recombination assay
  - Isolation of different stages of B cells using flow cytometry
  - Analysis of RAG1 expression following Dicer knockdown
  - Endogenous pulldown of AGO2 using immunoprecipitation assay
  - Argonaute HITS-CLIP to determine miR-29c interaction with RAG1 3′ UTR
- QUANTIFICATION AND STATISTICAL ANALYSIS

SUPPLEMENTAL INFORMATION

Supplemental information can be found online at https://doi.org/10.1016/j.celrep.2021.109390.

ACKNOWLEDGMENTS

We thank V. Gopalakrishnan, U. Ray, and other members of the SCR laboratory for discussions and comments on the manuscript. We thank S. Vartak and D. Dinesh for their help in cell culture. We thank the animal facility, IISc, and fluorescence-activated cell sorting (FACS) facility, IISc, for their help.

This work was supported by grants from DBT, India (Grant No. NO. BT/PR13616/GET/119/4/2015 and DT.4/1/2016) and COE (BT/PR13458/COE/34/33/2015) to S.C.R. and B.C. and financial assistance from IISc-DBT partnership program (DBT/BF/PR/INS/2011-12/IISc) to S.C.R. R.K. was supported by Senior Research fellowships from DBT and CSIR, India. U.R. is supported by a Senior Research Fellowship (SRF) from IISc.

AUTHOR CONTRIBUTIONS

S.C.R. and B.C. conceived and coordinated the study. S.C.R., B.C., K.N.B., M.N., R.K., U.R., S.D., and N.M.N. designed experiments. R.K., U.R., S.D., N.M.N., A.P., G.R., P.B., M.S., and B.C. performed experiments. S.C.R., B.C., R.K., U.R., and N.M.N. interpreted the data and wrote the paper.

DECLARATION OF INTERESTS

The authors declare no competing interests.

INCLUSION AND DIVERSITY

We worked to ensure sex balance in the selection of non-human subjects. We worked to ensure diversity in experimental samples through the selection of the cell lines.

Received: June 10, 2019
Revised: March 7, 2021
Accepted: June 22, 2021
Published: July 13, 2021

REFERENCES

Agarwal, V., Bell, G.W., Nam, J.W., and Bartel, D.P. (2015). Predicting effective microRNA target sites in mammalian mRNAs. eLife 4, e05005.

Ambros, V. (2004). The functions of animal microRNAs. Nature 431, 350–355.

Amin, R.H., and Schlissel, M.S. (2008). Foxo1 directly regulates the transcription of recombination-activating genes during B cell development. Nat. Immunol. 9, 613–622.

Barreto, V., Marques, R., and Demengeot, J. (2001). Early death and severe lymphopenia caused by ubiquitous expression of the Rag1 and Rag2 genes in mice. Eur. J. Immunol. 31, 3763–3772.

Besmer, E., Mansilla-Soto, J., Cassard, S., Sawchuk, D.J., Brown, G., Sadofsky, M., Lewis, S.M., Nussenzweig, M.C., and Cortes, P. (1998). Hairpin coding end opening is mediated by RAG1 and RAG2 proteins. Mol. Cell 2, 817–828.

Blume, C.J., Hotz-Wagenblatt, A., Hüllein, J., Sellner, L., Jethwa, A., Stolz, T., Slabicki, M., Lee, K., Sharathchandra, A., Benner, A., et al. (2015). p53-dependent non-coding RNA networks in chronic lymphocytic leukemia. Leukemia 29, 2015–2023.

Brown, S.T., Miranda, G.A., Galic, Z., Hartman, I.Z., Lyon, C.J., and Aguilera, R.J. (1997). Regulation of the RAG-1 promoter by the NF-Y transcription factor. J. Immunol. 158, 5071–5074.

Carmell, M.A., Xuan, Z., Zhang, M.Q., and Hannon, G.J. (2002). The Argonaute family: tentacles that reach into RNAi, developmental control, stem cell maintenance, and tumorigenesis. Genes Dev. 16, 2733–2742.

Chen, Z., Xiao, Y., Zhang, J., Li, J., Liu, Y., Zhao, Y., Ma, C., Luo, J., Qiu, Y., Huang, G., et al. (2011). Transcription factors E2A, FOXO1 and FOXP1 regulate recombination activating gene expression in cancer cells. PLoS ONE 6, e20475.

Chiruvella, K.K., Sebastian, R., Sharma, S., Karande, A.A., Choudhary, B., and Raghavan, S.C. (2012). Time-dependent predominance of nonhomologous DNA end-joining pathways during embryonic development in mice. J. Mol. Biol. 417, 197–211.

Coffre, M., Benhamou, D., Rieß, D., Blumenberg, L., Snetkova, V., Hines, M.J., Chakraborty, T., Bajwa, S., Jensen, K., Chong, M.M.W., et al. (2016). miRNAs Are Essential for the Regulation of the PI3K/AKT/FOXO Pathway and Receptor Editing during B Cell Maturation. Cell Rep. 17, 2271–2285.

Ding, D.P., Chen, Z.L., Zhao, X.H., Wang, J.W., Sun, J., Wang, Z., Tan, F.W., Tan, X.G., Li, B.Z., Zhou, F., et al. (2011). miR-29c induces cell cycle arrest in esophageal squamous cell carcinoma by modulating cyclin E expression. Carcinogenesis 32, 1025–1032.

Dong, X., Stothard, P., Forsythe, I.J., and Wishart, D.S. (2004). PlasMapper: a web server for drawing and auto-annotating plasmid maps. Nucleic Acids Res. 32, W660–W664.

Dooley, J., Garcia-Perez, J.E., Sreenivasan, J., Schlenner, S.M., Vangoitsenhoven, R., Papadopoulou, A.S., Tian, L., Schonefeldt, S., Serneels, L., Deroose, C., et al. (2016). The microRNA-29 Family Dictates the Balance Between Homeostatic and Pathological Glucose Handling in Diabetes and Obesity. Diabetes 65, 53–61.

Eastman, Q.M., Leu, T.M., and Schatz, D.G. (1996). Initiation of V(D)J recombination in vitro obeying the 12/23 rule. Nature 380, 85–88.

Ebert, P.J., Jiang, S., Xie, J., Li, Q.J., and Davis, M.M. (2009). An endogenous positively selecting peptide enhances mature T cell responses and becomes an autoantigen in the absence of microRNA miR-181a. Nat. Immunol. 10, 1162–1169.

Fabbri, M., Garzon, R., Cimmino, A., Liu, Z., Zanesi, N., Callegari, E., Liu, S., Alder, H., Costinean, S., Fernandez-Cymering, C., et al. (2007). MicroRNA-29 family reverts aberrant methylation in lung cancer by targeting DNA methyltransferases 3A and 3B. Proc. Natl. Acad. Sci. USA 104, 15805–15810.

Fernandes, R.C., Toubia, J., Townley, S., Hanson, A.R., Dredge, B.K., Pillman, K.A., Bert, A.G., Winter, J.M., Iggo, R., Das, R., et al.; MURAL investigators (2021). Post-transcriptional Gene Regulation by MicroRNA-194 Promotes Neuroendocrine Transdifferentiation in Prostate Cancer. Cell Rep. 34, 108585.

Fernandez-Mercado, M., Manterola, L., and Lawrie, C.H. (2015). MicroRNAs in Lymphoma: Regulatory Role and Biomarker Potential. Curr. Genomics 16, 349–358.

Garzon, R., Heaphy, C.E., Havelange, V., Fabbri, M., Volinia, S., Tsao, T., Zanesi, N., Kornblau, S.M., Marcucci, G., Calin, G.A., et al. (2009a). MicroRNA 29b functions in acute myeloid leukemia. Blood 114, 5331–5341.

Garzon, R., Liu, S., Fabbri, M., Liu, Z., Heaphy, C.E., Callegari, E., Schwind, S., Pang, J., Yu, J., Muthusamy, N., et al. (2009b). MicroRNA-29b induces global DNA hypomethylation and tumor suppressor gene reexpression in acute myeloid leukemia by targeting directly DNMT3A and 3B and indirectly DNMT1. Blood 113, 6411–6418.

Gauss, G.H., and Lieber, M.R. (1993). Unequal signal and coding joint formation in human V(D)J recombination. Mol. Cell. Biol. 13, 3900–3906.

Gebert, L.F.R., and MacRae, I.J. (2019). Regulation of microRNA function in animals. Nat. Rev. Mol. Cell Biol. 20, 21–37.

Gellert, M. (2002). V(D)J recombination: RAG proteins, repair factors, and regulation. Annu. Rev. Biochem. 71, 101–132.

Grawunder, U., Zimmer, D., Fugmann, S., Schwarz, K., and Lieber, M.R. (1998). DNA ligase IV is essential for V(D)J recombination and DNA double-strand break repair in human precursor lymphocytes. Mol. Cell 2, 477–484.

Griffiths-Jones, S. (2004). The microRNA Registry. Nucleic Acids Res. 32, D109–D111.

Haecker, I., Gay, L.A., Yang, Y., Hu, J., Morse, A.M., McIntyre, L.M., and Renne, R. (2012). Ago HITS-CLIP expands understanding of Kaposi's sarcoma-associated herpesvirus miRNA function in primary effusion lymphomas. PLoS Pathog. 8, e1002884.

Hammond, S.M., Caudy, A.A., and Hannon, G.J. (2001). Post-transcriptional gene silencing by double-stranded RNA. Nat. Rev. Genet. 2, 110–119.

Harayama, T., and Riezman, H. (2017). Detection of genome-edited mutant clones by a simple competition-based PCR method. PLoS One 12, e0179165.

Hines, M.J., Coffre, M., Mudianto, T., Panduro, M., Wigton, E.J., Tegla, C., Castro-Vasquez, V., Kageyama, R., Benhamou, D., Perez, O., et al. (2020). miR-29 Sustains B Cell Survival and Controls Terminal Differentiation via Regulation of PI3K Signaling. Cell Rep. 33, 108436.

Hirt, B. (1967). Selective extraction of polyoma DNA from infected mouse cell cultures. J. Mol. Biol. 26, 365–369.

Hsu, L.Y., Lauring, J., Liang, H.E., Greenbaum, S., Cado, D., Zhuang, Y., and Schlissel, M.S. (2003). A conserved transcriptional enhancer regulates RAG gene expression in developing B cells. Immunity 19, 105–117.

Ji, W., Sun, B., and Su, C. (2017). Targeting MicroRNAs in Cancer Gene Therapy. Genes (Basel) 8, 21.

Jiang, H., Zhang, G., Wu, J.H., and Jiang, C.P. (2014). Diverse roles of miR-29 in cancer (review). Oncol. Rep. 31, 1509–1516.

Jima, D.D., Zhang, J., Jacobs, C., Richards, K.L., Dunphy, C.H., Choi, W.W., Au, W.Y., Srivastava, G., Czader, M.B., Rizzieri, D.A., et al.; Hematologic Malignancies Research Consortium (2010). Deep sequencing of the small RNA transcriptome of normal and malignant human B cells identifies hundreds of novel microRNAs. Blood 116, e118–e127.

Jin, Z.X., Kishi, H., Wei, X.C., Matsuda, T., Saito, S., and Muraguchi, A. (2002). Lymphoid enhancer-binding factor-1 binds and activates the recombination-activating gene-2 promoter together with c-Myb and Pax-5 in immature B cells. J. Immunol. 169, 3783–3792.

Jin, Y., Chen, Z., Liu, X., and Zhou, X. (2013). Evaluating the microRNA targeting sites by luciferase reporter gene assay. Methods Mol. Biol. 936, 117–127.

Johnson, K., Chaumeil, J., and Skok, J.A. (2010). Epigenetic regulation of V(D)J recombination. Essays Biochem. 48, 221–243.

Kavitha, C.V., Nambiar, M., Ananda Kumar, C.S., Choudhary, B., Muniyappa, K., Rangappa, K.S., and Raghavan, S.C. (2009). Novel derivatives of spirohydantoin induce growth inhibition followed by apoptosis in leukemia cells. Biochem. Pharmacol. 77, 348–363.

Kavitha, C.V., Nambiar, M., Narayanaswamy, P.B., Thomas, E., Rathore, U., Ananda Kumar, C.S., Choudhary, B., Rangappa, K.S., and Raghavan, S.C. (2013). Propyl-2-(8-(3,4-difluorobenzyl)-2′,5′-dioxo-8-azaspiro[bicyclo[3.2.1] octane-3,4′-imidazolidine]-1′-yl) acetate induces apoptosis in human leukemia cells through mitochondrial pathway following cell cycle arrest. PLoS ONE 8, e69103.

Ketting, R.F., Fischer, S.E., Bernstein, E., Sijen, T., Hannon, G.J., and Plasterk, R.H. (2001). Dicer functions in RNA interference and in synthesis of small RNA involved in developmental timing in C. elegans. Genes Dev. 15, 2654–2659.

Kim, V.N. (2005). MicroRNA biogenesis: coordinated cropping and dicing. Nat. Rev. Mol. Cell Biol. 6, 376–385.

Kishi, H., Jin, Z.X., Wei, X.C., Nagata, T., Matsuda, T., Saito, S., and Muraguchi, A. (2002). Cooperative binding of c-Myb and Pax-5 activates the RAG-2 promoter in immature B cells. Blood 99, 576–583.

Koralov, S.B., Muljo, S.A., Galler, G.R., Krek, A., Chakraborty, T., Kanellopoulou, C., Jensen, K., Cobb, B.S., Merkenschlager, M., Rajewsky, N., and Rajewsky, K. (2008). Dicer ablation affects antibody diversity and cell survival in the B lymphocyte lineage. Cell 132, 860–874.

Kouzine, F., Wojtowicz, D., Yamane, A., Resch, W., Kieffer-Kwon, K.R., Bandle, R., Nelson, S., Nakahashi, H., Awasthi, P., Feigenbaum, L., et al. (2013). Global regulation of promoter melting in naive lymphocytes. Cell 153, 988–999.

Kuchen, S., Resch, W., Yamane, A., Kuo, N., Li, Z., Chakraborty, T., Wei, L., Laurence, A., Yasuda, T., Peng, S., et al. (2010). Regulation of microRNA expression and abundance during lymphopoiesis. Immunity 32, 828–839.

Kuo, T.C., and Schlissel, M.S. (2009). Mechanisms controlling expression of the RAG locus during lymphocyte development. Curr. Opin. Immunol. 21, 173–178.

Kwon, J.J., Factora, T.D., Dey, S., and Kota, J. (2019). A Systematic Review of miR-29 in Cancer. Mol. Ther. Oncolytics 12, 173–194.

Landgraf, P., Rusu, M., Sheridan, R., Sewer, A., Iovino, N., Aravin, A., Pfeffer, S., Rice, A., Kamphorst, A.O., Landthaler, M., et al. (2007). A mammalian microRNA expression atlas based on small RNA library sequencing. Cell 129, 1401–1414.

Langmead, B., and Salzberg, S.L. (2012). Fast gapped-read alignment with Bowtie 2. Nat. Methods 9, 357–359.

Lauring, J., and Schlissel, M.S. (1999). Distinct factors regulate the murine RAG-2 promoter in B- and T-cell lines. Mol. Cell. Biol. 19, 2601–2612.

Lee, J., and Desiderio, S. (1999). Cyclin A/CDK2 regulates V(D)J recombination by coordinating RAG-2 accumulation and DNA repair. Immunity 11, 771–781.

Lee, B.S., Lee, B.K., Iyer, V.R., Sleckman, B.P., Shaffer, A.L., 3rd, Ippolito, G.C., Tucker, H.O., and Dekker, J.D. (2018). Corrected and Republished from: BCL11A Is an Integral Component of a Transcriptional Network That Activates RAG Expression and V(D)J Recombination. Mol. Cell. Biol. 38, e00362-17.

Lewis, S.M., Agard, E., Suh, S., and Czyzyk, L. (1997). Cryptic signals and the fidelity of V(D)J joining. Mol. Cell. Biol. 17, 3125–3136.

Li, Z., Dordai, D.I., Lee, J., and Desiderio, S. (1996). A conserved degradation signal regulates RAG-2 accumulation during cell division and links V(D)J recombination to the cell cycle. Immunity 5, 575–589.

Li, Q.J., Chau, J., Ebert, P.J., Sylvester, G., Min, H., Liu, G., Braich, R., Manoharan, M., Soutschek, J., Skare, P., et al. (2007). miR-181a is an intrinsic modulator of T cell sensitivity and selection. Cell 129, 147–161.

Li, H., Handsaker, B., Wysoker, A., Fennell, T., Ruan, J., Homer, N., Marth, G., Abecasis, G., and Durbin, R.; 1000 Genome Project Data Processing Subgroup (2009). The Sequence Alignment/Map format and SAMtools. Bioinformatics 25, 2078–2079.

Lieber, M.R., Hesse, J.E., Mizuuchi, K., and Gellert, M. (1988). Studies of V(D)J recombination with extrachromosomal substrates. Curr. Top. Microbiol. Immunol. 137, 94–99.

Liston, A., Papadopoulou, A.S., Danso-Abeam, D., and Dooley, J. (2012). MicroRNA-29 in the adaptive immune system: setting the threshold. Cell. Mol. Life Sci. 69, 3533–3541.

Malu, S., Malshetty, V., Francis, D., and Cortes, P. (2012). Role of non-homologous end joining in V(D)J recombination. Immunol. Res. 54, 233–246.

Marcucci, G., Maharry, K.S., Metzeler, K.H., Volinia, S., Wu, Y.Z., Mrózek, K., Nicolet, D., Kohlschmidt, J., Whitman, S.P., Mendler, J.H., et al. (2013). Clinical role of microRNAs in cytogenetically normal acute myeloid leukemia: miR-155 upregulation independently identifies high-risk patients. J. Clin. Oncol. 31, 2086–2093.

Mi, S., Lu, J., Sun, M., Li, Z., Zhang, H., Neilly, M.B., Wang, Y., Qian, Z., Jin, J., Zhang, Y., et al. (2007). MicroRNA expression signatures accurately discriminate acute lymphoblastic leukemia from acute myeloid leukemia. Proc. Natl. Acad. Sci. USA 104, 19971–19976.

Mizuta, R., Mizuta, M., Araki, S., and Kitamura, D. (2002). RAG2 is down-regulated by cytoplasmic sequestration and ubiquitin-dependent degradation. J. Biol. Chem. 277, 41423–41427.

Naik, A.K., Lieber, M.R., and Raghavan, S.C. (2010). Cytosines, but not purines, determine recombination activating gene (RAG)-induced breaks on heteroduplex DNA structures: implications for genomic instability. J. Biol. Chem. 285, 7587–7597.

Nambiar, M., and Raghavan, S.C. (2011). How does DNA break during chromosomal translocations? Nucleic Acids Res. 39, 5813–5825.

Nambiar, M., and Raghavan, S.C. (2012). Mechanism of fragility at BCL2 gene minor breakpoint cluster region during t(14;18) chromosomal translocation. J. Biol. Chem. 287, 8688–8701.

Nambiar, M., Goldsmith, G., Moorthy, B.T., Lieber, M.R., Joshi, M.V., Choudhary, B., Hosur, R.V., and Raghavan, S.C. (2011). Formation of a G-quadruplex at the BCL2 major breakpoint region of the t(14;18) translocation in follicular lymphoma. Nucleic Acids Res. 39, 936–948.

Nishana, M., and Raghavan, S.C. (2012). Role of recombination activating genes in the generation of antigen receptor diversity and beyond. Immunology 137, 271–281.

Patnaik, P.K., Kulkarni, S.K., and Cross, G.A. (1993). Autonomously replicating single-copy episomes in Trypanosoma brucei show unusual stability. EMBO J. 12, 2529–2538.

Pekarsky, Y., Santanam, U., Cimmino, A., Palamarchuk, A., Efanov, A., Maximov, V., Volinia, S., Alder, H., Liu, C.G., Rassenti, L., et al. (2006). Tcl1 expression in chronic lymphocytic leukemia is regulated by miR-29 and miR-181. Cancer Res. 66, 11590–11593.

Pieper, K., Grimbacher, B., and Eibel, H. (2013). B-cell biology and development. J. Allergy Clin. Immunol. 131, 959–971.

Pfeifer, P., Holla, S., Ghorpade, D.S., [illegible], and Balaji, K.N. (2013). [illegible] responsive miR-132 and miR-146 target receptor-interacting protein kinase 2 and transforming growth factor beta-activated kinase 1 to suppress NOD2-induced immunomodulation. J. Biol. Chem. 288, 25375–25386.

Quinlan, A.R., and Hall, I.M. (2010). BEDTools: a flexible suite of utilities for comparing genomic features. Bioinformatics 26, 841–842.

Raghavan, S.C., Kirsch, I.R., and Lieber, M.R. (2001). Analysis of the V(D)J recombination efficiency at lymphoid chromosomal translocation breakpoints. J. Biol. Chem. 276, 29126–29133.

Raghavan, S.C., Swanson, P.C., Wu, X., Hsieh, C.L., and Lieber, M.R. (2004). A non-B-DNA structure at the Bcl-2 major breakpoint region is cleaved by the RAG complex. Nature 428, 88–93.

Raghavan, S.C., Swanson, P.C., Ma, Y., and Lieber, M.R. (2005). Double-strand break formation by the RAG complex at the bcl-2 major breakpoint region and at other non-B DNA structures in vitro. Mol. Cell. Biol. 25, 5904–5919.

Ran, F.A., Hsu, P.D., Wright, J., Agarwala, V., Scott, D.A., and Zhang, F. (2013). Genome engineering using the CRISPR-Cas9 system. Nat. Protoc. 8, 2281–2308.

Rand, T.A., Ginalski, K., Grishin, N.V., and Wang, X. (2004). Biochemical identification of Argonaute 2 as the sole protein required for RNA-induced silencing complex activity. Proc. Natl. Acad. Sci. USA 101, 14385–14389.

Robinson, J.T., Thorvaldsdóttir, H., Winckler, W., Guttman, M., Lander, E.S., Getz, G., and Mesirov, J.P. (2011). Integrative genomics viewer. Nat. Biotechnol. 29, 24–26.

Roth, D.B. (2003). Restraining the V(D)J recombinase. Nat. Rev. Immunol. 3, 656–666.

Rudin, C.M., and Thompson, C.B. (1998). B-cell development and maturation. Semin. Oncol. 25, 435–446.

Sanjana, N.E., Shalem, O., and Zhang, F. (2014). Improved vectors and genome-wide libraries for CRISPR screening. Nat. Methods 11, 783–784.

Schatz, D.G., and Ji, Y. (2011). Recombination centres and the orchestration of V(D)J recombination. Nat. Rev. Immunol. 11, 251–263.

Schatz, D.G., and Swanson, P.C. (2011). V(D)J recombination: mechanisms of initiation. Annu. Rev. Genet. 45, 167–202.

Schlissel, M.S. (2003). Regulating antigen-receptor gene assembly. Nat. Rev. Immunol. 3, 890–899.

Sebastian, R., and Raghavan, S.C. (2015). Endosulfan induces male infertility. Cell Death Dis. 6, e2022.

Shah, M.Y., Ferrajoli, A., Sood, A.K., Lopez-Berestein, G., and Calin, G.A. (2016). microRNA Therapeutics in Cancer - An Emerging Concept. EBioMedicine 12, 34–42.

Sharma, S., Choudhary, B., and Raghavan, S.C. (2011). Efficiency of nonhomologous DNA end joining varies among somatic tissues, despite similarity in mechanism. Cell. Mol. Life Sci. 68, 661–676.

Sharma, S., Javadekar, S.M., Pandey, M., Srivastava, M., Kumari, R., and Raghavan, S.C. (2015). Homology and enzymatic requirements of microhomology-dependent alternative end joining. Cell Death Dis. 6, e1697.

Shockett, P.E., and Schatz, D.G. (1999). DNA hairpin opening mediated by the RAG1 and RAG2 proteins. Mol. Cell. Biol. 19, 4159–4166.

Singh, A., Manjunath, L.E., Kundu, P., Sahoo, S., Das, A., Suma, H.R., Fox, P.L., and Eswarappa, S.M. (2019). Let-7a-regulated translational readthrough of mammalian AGO1 generates a microRNA pathway inhibitor. EMBO J. 38, e100727.

Solé, C., Larrea, E., Di Pinto, G., Tellaetxe, M., and Lawrie, C.H. (2017). miRNAs in B-cell lymphoma: Molecular mechanisms and biomarker potential. Cancer Lett. 405, 79–89.

Solé, C., Arnaiz, E., and Lawrie, C.H. (2018). MicroRNAs as Biomarkers of B-cell Lymphoma. Biomark. Insights 13, 1177271918806840.

Thomas, M.D., Srivastava, B., and Allman, D. (2006). Regulation of peripheral B cell maturation. Cell. Immunol. 239, 92–102.

van Gent, D.C., Ramsden, D.A., and Gellert, M. (1996). The RAG1 and RAG2 proteins establish the 12/23 rule in V(D)J recombination. Cell 85, 107–113.

Verboom, K., Van Loocke, W., Volders, P.J., Decaesteker, B., Cobos, F.A., Bornschein, S., de Bock, C.E., Atak, Z.K., Clappier, E., Aerts, S., et al. (2018). A comprehensive inventory of TLX1 controlled long non-coding RNAs in T-cell acute lymphoblastic leukemia through polyA+ and total RNA sequencing. Haematologica 103, e585–e589.

Wallaert, A., Van Loocke, W., Hernandez, L., Taghon, T., Speleman, F., and Van Vlierberghe, P. (2017). Comprehensive miRNA expression profiling in human T-cell acute lymphoblastic leukemia by small RNA-sequencing. Sci. Rep. 7, 7901.

Wang, X. (2008). miRDB: a microRNA target prediction and functional annotation database with a wiki interface. RNA 14, 1012–1017.

Wang, Q.F., Lauring, J., and Schlissel, M.S. (2000). c-Myb binds to a sequence in the proximal region of the RAG-2 promoter and is essential for promoter activity in T-lineage cells. Mol. Cell. Biol. 20, 9203–9211.

Wang, X.S., Gong, J.N., Yu, J., Wang, F., Zhang, X.H., Yin, X.L., Tan, Z.Q., Luo, Z.M., Yang, G.H., Shen, C., and Zhang, J.W. (2012). MicroRNA-29a and microRNA-142-3p are regulators of myeloid differentiation and acute myeloid leukemia. Blood 119, 4992–5004.

Wang, J., Chen, J., and Sen, S. (2016). MicroRNA as Biomarkers and Diagnostics. J. Cell. Physiol. 231, 25–30.

Xiong, Y., Fang, J.H., Yun, J.P., Yang, J., Zhang, Y., Jia, W.H., and Zhuang, S.M. (2010). Effects of microRNA-29 on apoptosis, tumorigenicity, and prognosis of hepatocellular carcinoma. Hepatology 51, 836–845.

Yamane, A., Resch, W., Kuo, N., Kuchen, S., Li, Z., Sun, H.W., Robbiani, D.F., McBride, K., Nussenzweig, M.C., and Casellas, R. (2011). Deep-sequencing identification of the genomic targets of the cytidine deaminase AID and its cofactor RPA in B lymphocytes. Nat. Immunol. 12, 62–69.

Zhao, J.J., Lin, J., Lwin, T., Yang, H., Guo, J., Kong, W., Dessureault, S., Moscinski, L.C., Rezania, D., Dalton, W.S., et al. (2010). microRNA expression profile and identification of miR-29 as a prognostic marker and pathogenetic factor by targeting CDK6 in mantle cell lymphoma. Blood 115, 2630–2639.

Zheng, R.L., Jiang, Y.J., and Wang, X. (2014). Role of microRNAs on therapy resistance in Non-Hodgkin's lymphoma. Int. J. Clin. Exp. Med. 7, 3818–3832.

Zhou, B., Wang, S., Mayr, C., Bartel, D.P., and Lodish, H.F. (2007). miR-150, a microRNA expressed in mature B and T cells, blocks early B cell development when expressed prematurely. Proc. Natl. Acad. Sci. USA 104, 7080–7085. https://doi.org/10.1073/pnas.0702409104.

STAR★METHODS

KEY RESOURCES TABLE

REAGENT or RESOURCE	SOURCE	IDENTIFIER
Antibodies		
RAG-1 Antibody (K-20)	Santa Cruz Biotechnology	Cat# sc-363; RRID: AB_632307
RAG-1 Antibody (D-5)	Santa Cruz Biotechnology	Cat# sc-377127
RAG-2 (M-300) antibody	Santa Cruz Biotechnology	Cat# sc-5600; RRID: AB_655069
AGO2 antibody	Cusabio Technology	Sandeep M. Eswarappa, IISc, Bangalore Cat# CSB-PA891731LA01HU
Dicer1 human antibody	Sigma Aldrich	Sandeep M. Eswarappa, IISc, Bangalore (Singh et al., 2011) Cat# SAB4200087; RRID: AB_10603338
α-Tubulin Antibody	Cell Signaling Technology	Cat# 2144S; RRID: AB_2210548
PCNA (F-2) antibody	Santa Cruz Biotechnology	Cat# sc-25280; RRID: AB_628109
GAPDH (A-3) antibody	Santa Cruz Biotechnology	Cat# sc-137179; RRID: AB_2232048
APC Rat Anti Mouse CD45	BD Biosciences	Cat# 559864; RRID: AB_398672
PE-Cy7 Rat Anti-Mouse CD25	BD Biosciences	Cat# 552880; RRID: AB_394509
FITC Rat Anti-Mouse CD43	BD Biosciences	Cat# 553270; RRID: AB_394747
FITC Rat Anti-Mouse IgD	BD Biosciences	Cat# 562022; RRID: AB_10894208
PE-Cy7 Rat Anti-Mouse IgM	BD Biosciences	Cat# 552867; RRID: AB_394500
Mouse anti-rabbit IgG-B	Santa Cruz Biotechnology	Cat# sc-2491; RRID: AB_628495
Goat anti-mouse IgG-HRP	Santa Cruz Biotechnology	Cat# sc-2005; RRID: AB_631736
Goat anti-mouse IgG-B	Santa Cruz Biotechnology	Cat# sc-2039; RRID: AB_631734
Mouse anti-rabbit IgG-HRP	Santa Cruz Biotechnology	Cat# sc-2357; RRID: AB_628497
m-IgGκ BP-HRP Antibody	Santa Cruz Biotechnology	Cat# sc-516102; RRID: AB_2687626
Protein A/G PLUS-Agarose antibody	Santa Cruz Biotechnology	Cat# sc-2003; RRID: AB_10201400
HRP-Streptavidin	Sigma Aldrich	Cat# RABHRP3
Bacterial and virus strains		
E. coli DH5α	Prof. Umesh Varshney, IISc, Bangalore	N/A
E. coli DH10β	Prof. K. Muniyappa, IISc, Bangalore	N/A
Chemicals, peptides, and recombinant proteins		
TRI reagent	Sigma Aldrich	Cat# 93289
*mir*Vana miRNA Inhibitor	Invitrogen	Cat# 4464084
o-Nitrophenyl-β-D-galactopyranoside	HIMEDIA	Cat# RM582
OptiMEM Reduced Serum Medium	GIBCO	Cat# 31985062
Linear Polyethylenimine	Polysciences	Cat# 23966-2
Puromycin dihydrochloride	Sigma Aldrich	Cat# P8833
Lipofectamine 2000	Invitrogen	Cat# 11668019
Immobilon Forte Western HRP Substrate	Merck Millipore	Cat# WBLUF0100
Critical commercial assays		
GenElute Gel Extraction Kit	Sigma Aldrich	Cat# NA1111
Luciferase Assay System with Reporter Lysis Buffer	Promega	Cat# E4030
SybrGreen master mix	Biorad	Cat# 1725124
TB Green Premix Ex Taq II	TaKaRa	Cat # RR820B
T4 DNA Ligase	NEB	Cat# M0201L
M-MuLV Reverse Transcriptase	NEB	Cat# M0253S
TA vector	Thermo Fisher Scientific	Cat# 450030

(Continued on next page)

Continued

REAGENT or RESOURCE	SOURCE	IDENTIFIER
BsmBI	NEB	Cat# R0739S
Proteinase K	SRL	Cat# 1548179
DNaseI	NEB	Cat# M0303S
Experimental models: Cell lines		
CEM	NCCS, Pune	N/A
Nalm6	Dr. Michael R. Lieber, University of Southern California	N/A
Reh	Dr. Michael R. Lieber	N/A
Raji	NCCS, Pune	N/A
SUDHL8	Dr. Alan L. Epstein, University of Southern California	N/A
Jurkat	NCCS, Pune	N/A
N114	Dr. Michael R. Lieber	[Qiaosimor et al., 1993]
SupT1	NCCS, Pune	N/A
K562	NCCS, Pune	N/A
N6-29c-B5	This paper	N/A
Experimental models: Organisms/strains		
miR29c−/− mice	[Oakley et al., 2011]	N/A
C57BL/6 mice	Central Animal Facility, IISc, Bangalore	N/A
BALB/c mice	Central Animal Facility, IISc, Bangalore	N/A
Oligonucleotides		
Primer: 18S rRNA Forward (SS46) 5′-TCC ATTGGAGGGCAAGT-3′	IDT	N/A
Primer: 18S rRNA Reverse (SS47) 5′-ACG AGCTTTTTAACTGCAGCAA-3′	IDT	N/A
Primer: pre-miR-29c Forward (RK70) 5′-CTCGAGCCATTAAACTATCTCTT ACCTCTGC-3′	IDT	N/A
Primer: pre-miR-29c Reverse (RK71) 5′-GAATTCGACTCCTAGCAGCCAT CACC-3′	IDT	N/A
Primer: miR-29c-3p Forward (RK68) 5′-CGCCCACTATAACCACCAACAT-3′	IDT	N/A
Primer: miR-29c-3p Reverse (RK73) 5′-CGTTCCATTAGCACCATTTGAA-3′	IDT	N/A
Adaptor primer: Forward (RK66) 5′-CGTTCCATTGACCGATTTCTCCT-3′	IDT	N/A
Adaptor primer: Reverse (RK72) 5′-CGCCCACTATAACCACCA ACATTAACCGAT-3′	IDT	N/A
Primer: 3′UTR-RAG1 Forward (RK84) 5′-GACGAATTCCCTAACCCTCTTG TGGCTCC-3′	IDT	N/A
Primer: 3′UTR-RAG1 Reverse (RK85) 5′-TATTCTAGAGGAAAGTGTGGCTT AGTGGC-3′	IDT	N/A
Primer: Forward (RK90) 5′-ATGTAT TTAGCGATTCTTCAGG-3′	IDT	N/A
Primer: Reverse (RK91) 5′-CCTGA AGAATCGCTAAATACAT-3′	IDT	N/A
Primer: HPRT Forward (KKC11) 5′-GCCTGTATCCAACACTTCG-3′	IDT	N/A

(Continued on next page)

Continued

REAGENT or RESOURCE	SOURCE	IDENTIFIER
Primer: HPRT Reverse (KK012) 5'-AGCG TCGTGATTAGCGATG-3'	IDT	N/A
Primer: RAG2 Forward (AP21) 5'-CTGC CCTACTTGTGATGTGG-3'	IDT	N/A
Primer: RAG2 Reverse (AP22) 5'-GATG GATGAGTGTGCGTTCT-3'	IDT	N/A
Primer: RAG1 Forward #1 (AP19) 5'-GG CTTCTGGCTCAGTCTACA-3'	IDT	N/A
Primer: RAG1 Reverse #1 (AP20) 5'-CT CAGCATGGCTTCTGGTTA-3'	IDT	N/A
Primer: RAG1 Forward #2 (AP32) 5'-CC GTGTCAACACCTTCCTCA-3'	IDT	N/A
Primer: RAG1 Reverse #2 (AP33) 5'-TC CCATGCTTCTCACTCACG-3'	IDT	N/A
Primer: RAG1 Forward #3 (NMN9) 5'-CC GTGTCAATACCTTCCTCA-3'	Eurofins Scientific	N/A
Primer: RAG1 Reverse #3 (NMN10) 5'-CC GTGTCAATACCTTCCTCA-3'	Eurofins Scientific	N/A
Primer: RAG1 Forward #4 (NMN85) 5'-TG GCAATGTAGAGCAGGCAT-3'	Juniper	N/A
Primer: RAG1 Reverse #4 (NMN86) 5'-AG TGCAGAGACATGCTGGAA-3'	Juniper	N/A
Primer: RAG1 Reverse #5 (NMN89) 5'-GT TCAATCCCTGAAGAAGCACC-3'	Juniper	N/A
Primer: RAG1 (mouse) Forward (RK3) 5'CGACCAGAATAACCACCAACATA GAATCCT 3'	IDT	N/A
Primer: RAG1 (mouse) Reverse (SS10) 5'-CAACATCTGCCTTCACGTCGATCC-3'	IDT	N/A
Primer: LHR Forward (LHRF1) 5'-AGCT TGGGATTACATTTTTATGGGGCA-3'	IDT	N/A
Primer: LHR Reverse (LHRR1) 5'-TAAC TGAAGAATCGCTAAATACAT-3'	IDT	N/A
Primer: RHR Forward (RHRF1) 5'-ATGTATTTAGCGATTCTTCAGTTA-3'	IDT	N/A
Primer: RHR Reverse (RHRR2) 5'-TCGAG AATCATGCTCTTAGTCACATGC-3	IDT	N/A

Recombinant DNA

pmirGLO plasmid	Promega	Cat# E1330
lentiCRISPR v2 plasmid	Addgene	RRID: Addgene_52961
β-galactosidase plasmid	Dr. K Somasundaram, IISc, Bangalore	N/A
pGG51 plasmid	Dr. Michael R. Lieber	(Gauss and Lieber, 1992)
pcDNA3.1 mRFP plasmid	Dr. Arun Kumar, IISc Bangalore	N/A
pGG49 plasmid	Dr. Michael R. Lieber	(Gauss and Lieber, 1992)
pMIR-RECK-3'UTR plasmid	Addgene	RRID: Addgene_53814
pBluescript (SK+) vector	Agilent	Cat# 212205
pIRES2-EGFP plasmid	BD Biosciences, Clontech	Cat #6029-1
pRK3 plasmid	This paper	N/A
pRK4 plasmid	This paper	N/A
pRK9 plasmid	This paper	N/A
pRK10 plasmid	This paper	N/A
pRK12 plasmid	This paper	N/A

(Continued on next page)

Continued

REAGENT or RESOURCE	SOURCE	IDENTIFIER
pRK13 plasmid	This paper	N/A
pRK15 plasmid	This paper	N/A
pRK17 plasmid	This paper	N/A
pMS51 plasmid	This paper	N/A
pMS52 plasmid	This paper	N/A
pMS53 plasmid	This paper	N/A
shRNA (DICER1)	shRNA Resource Center at Division of Biological Science, IISc, Bangalore	TRCN0000290426 and TRCN0000290488
Software and algorithms		
Prism 7.0	GraphPad Software	RRID:SCR_002798
FlasMapper Version 2.0	(Dong et al., 2004)	http://wishart.biology.ualberta.ca/FlasMapper/
SnapGene Viewer	https://www.snapgene.com/snapgene-viewer/	RRID:SCR_015053
Multigauge Version 3.0	Multigauge software	N/A
BD FACS DIVA software version 6.1.3	https://www.bdbiosciences.com/en-in	N/A
miRBase	(Griffiths-Jones, 2004)	http://www.mirbase.org/
miRDB	(Wang, 2008)	http://mirdb.org/index.html
TargetScan 7.2	(Agarwal et al., 2015)	http://www.targetscan.org/vert_72/
Bowtie2	(Langmead and Salzberg, 2012)	http://bowtie-bio.sourceforge.net/bowtie2/index.shtml
SAMtools	(Li et al., 2009)	http://samtools.sourceforge.net/
BEDtools	(Quinlan and Hall, 2010)	https://bedtools.readthedocs.io/en/latest/
IGV	(Robinson et al., 2011)	https://software.broadinstitute.org/software/igv/home
Other		
DNA sequencing	Medauxin, Amnion Biosciences and SciGenom, India	N/A
SRP002412	(Kuchen et al., 2010; Kuchen et al., 2011; Yamane et al., 2011)	https://www.ncbi.nlm.nih.gov/sra/?term=SRP002412
SRP000729	(Jima et al., 2010)	https://www.ncbi.nlm.nih.gov/pmc/articles/PMC2913999/
SRP002958	(Kuchen et al., 2010)	https://www.ncbi.nlm.nih.gov/sra/?term=SRP002958
GSE56156	(Khan et al., 2015)	https://www.ncbi.nlm.nih.gov/geo/query/acc.cgi?acc=GSE56156
GSE89978	(Willett et al., 2017)	https://www.ncbi.nlm.nih.gov/geo/query/acc.cgi
GSE110637	(Verboom et al., 2018)	https://www.ncbi.nlm.nih.gov/geo/query/acc.cgi
GSE137071	(Fernandes et al., 2021)	https://www.ncbi.nlm.nih.gov/geo/query/acc.cgi?acc=GSE137071

RESOURCE AVAILABILITY

Lead contact

Further information and requests for resources and reagents should be directed to and will be fulfilled by the Lead contact, Dr. Sathees C. Raghavan, Department of Biochemistry, Indian Institute of Science, Bangalore 560012. (sathees@iisc.ac.in)

Materials availability

Plasmids (pRK3, pRK4, pRK9, pRK10, pRK12, pRK13, pRK17, pRK15, pMS51, pMS52 and pMS53) and N6-29c-B5 cell line (mutation at the miR-29c binding site of *RAG1* 3′UTR) generated in this study will be made available on request. Transfer may require completion of material transfer agreement.

There are restrictions to the availability of miR-29c −/− mice generated by research group of Dr. Adnan Liston as the mice were culled after completion of their study.

Data and code availability

This study did not generate any new datasets or codes.

EXPERIMENTAL MODEL AND SUBJECT DETAILS

Animals

For the *in vivo* animal studies, B cells were isolated and sorted from 4-8 weeks old BALB/c (male) or C57BL/6 mice (male). Mice were housed and maintained as per the guidelines of the ethical committee for animal care, Indian Institute of Science in accordance with Indian National Law on animal care and use. The animals were housed in polypropylene cages and provided standard pellet diet (Agro Corporation Pvt. Ltd., India) and water *ad libitum*. They were maintained in optimum temperature and humidity with a 12 h light/dark cycle (Sebastian and Raghavan, 2015).

For generation of miR-29c −/− mice, the locus for miR-b2/c was designed such that two loxP* (modified) sites are inserted between NheI and SphI sites. The construct was then transfected into mice embryos. These were then crossed with EIIA-Cre mice, wherein the floxed genes were lost and miR-b2/c −/− mice (male and female) were generated (Dooley et al., 2010).

Cell lines

The cell lines used in the current study include Reh, Raji, SUDHL8, CEM, Jurkat, SupT1, Nalm6, N114 and K562. CEM, Nalm6, N114 (Greaves et al., 1999) and Reh cells were from Dr. M. Lieber (USA). SUDHL8 is a kind gift from Dr. A. Epstein, USA. K562, Raji and Jurkat cells were purchased from National Center for Cell Science, Pune, India. All cell lines were cultured in RPMI 1640 media supplemented with 10% FBS, 100 U Penicillin G/ml and 100 μg/ml of streptomycin (Sigma Aldrich, USA). Cells were cultured by incubating at 37° C in a humidified atmosphere containing 5% CO_2. The cell line N6-29c-B5 was generated during this study.

METHOD DETAILS

Enzymes, chemicals and reagents

Chemical reagents used in the study were bought from Sigma Chemical Co. (St. Louis, MO), and SRL (India). Restriction enzymes and DNA modifying enzymes were from New England Biolabs (Beverly, MA). Culture media were purchased from Sera Laboratory International Limited (West Sussex, UK) and Lonza (Basel, Switzerland). Fetal bovine serum (FBS) and PenStrep were purchased from GIBCO-BRL (USA). Antibodies were from Santa Cruz Biotechnology (USA), Sigma Aldrich (USA), Cell Signaling Technology (USA) and BD Biosciences (India). Gel elution kit was purchased from Sigma Aldrich (USA) and QIAGEN (Germany). Luciferase assay kit was from Promega (Madison, USA).

Plasmids

The plasmid pmirGLO (luciferase vector) was purchased from Promega (Madison, USA). Expression vector pIRES2-EGFP and β-galactosidase were kind gifts from Dr. K. Somasundaram, India. V(D)J recombination constructs, pGG51 and pGG49 were gifts from Dr. M. Lieber, USA (Gauss and Lieber, 1993). Plasmid DNA pcDNA3.1 mRFP was a kind gift from Dr. Arun Kumar, India. Lenti-CRISPRv2 was a gift from Feng Zhang (Addgene plasmid # 52961; http://www.addgene.org/52961; RRID:Addgene_52961)

Datasets for miRNA studies

Small RNA-seq datasets from NCBI public repository with accession ID SRA: SRP002412 (mouse) (Koutsos et al., 2013; Kuchen et al., 2010; Yamane et al., 2014), SRA: SRP002958 (human) (Kuchen et al., 2010) and SRA: SRP000729 (human) (Jima et al., 2010) were downloaded from NCBI SRA (sequence read archive) and used for the study. We considered dataset derived from samples of pro-B, pre-B, immature and mature B cell stages in case of mouse, while it was from centrocytes, pre-GCB, plasma, naive and memory B cells from human, along with various leukemia/lymphoma cell lines. miRDB (Wang, 2008) and TargetScan 7.2 (Agarwal et al., 2015), two of the well-known miRNA specific databases were considered for prediction of miRNA that target the 3'UTR of *RAG1*. To do this, the 3'UTR fasta sequence of RAG1 was submitted to the custom prediction tools of above-mentioned databases. The predicted miRNAs based on the analysis were further checked for their expression levels across the different stages of B cell development based on small RNA-seq data derived from specified SRPs (Robinson et al., 2011).

Method used to compute transcript expression

The raw reads from the datasets were checked for their quality using the FastQC tool. Reads with a phred quality score of less than Q30 were trimmed from both 5' and 3' end, minimum of 18 nucleotides from an initial read length of 25-36 nucleotides. Post trimming the reads were mapped to the mouse reference (mm10) and human reference (hg38) genome, respectively using the Bowtie2 aligner (Langmead and Salzberg, 2012). The resulting SAM files were compressed and sorted into their binary BAM formats using the SAMtools package (Li et al., 2009). Further, the read counts per miRNA transcript were obtained using the BEDtools suite (Quinlan and

Hall, 2010). The read counts were normalized by using the RPM method, i.e., RPM = number of reads mapped per transcript/ (total number of mapped reads /10^6). The rpm values were extracted and a heatmap was plotted in R using the pheatmap package.

T-ALL and CLL patients' datasets used to study miRNA and RAG1 expression

Normalized Read count files for miRNA transcripts and mRNA transcripts from 15 CLL patients were downloaded from GEO dataset GEO: GSE66186 (Blume et al., 2015). Raw read count files for miRNA and mRNA transcripts for 48 T-ALL patients were downloaded from GEO datasets GEO: GSE89978 and GEO: GSE110637, respectively (Verboom et al., 2018; Vaillant et al., 2017). RPM values for miRNA and RPKM values for mRNA were calculated for both the datasets using the following formulae, RPM = read count/ (total number of reads mapped/10^6) and RPKM = read count / (transcript length/1000) *(total number of reads mapped /10^6). The normalized values for miR-29c-3p and RAG1 were plotted in a heatmap using the pheatmap package in R.

RNA isolation and preparation of cDNA

RNA was prepared from cell lines or tissues using TRI reagent (Sigma-Aldrich) as per the manufacturer's instructions. Total RNA was isolated from different lymphoid and nonlymphoid cell lines (Nalm6, Reh, Raji, SUDHL8, CEM, Jurkat, SupT1 and K562) as well as mouse tissues (brain, heart, kidney, liver, lung, spleen, testis, and thymus).

Cells or tissues were homogenized with pestle at 4°C, chloroform was added, mixed vigorously and incubated on ice (10 min). Following centrifugation (12,000 rpm, 20 min at 4°C), equal volume of isopropanol was added to the supernatant, mixed and centrifuged (14,000 rpm, 30 min at 4°C). Pellet was ethanol washed, dried and resuspended in DEPC treated, autoclaved, double-distilled H_2O. Quality of the RNA was checked on agarose gel (1%) and quantitated using Nanodrop.

~5 μg of RNA was used for cDNA preparation. Following DNase treatment of RNA samples (10 min at 37°C), cDNA was prepared using M-MuLV Reverse Transcriptase (1 h at 37°C) using whole RNA, random hexamer and oligo$(dT)_{18}$. For amplification of miR-29c-3p, adaptor primers RK66/RK72 were added. First, adaptor primers were added to each of the samples and incubated at 37°C for 30 min, followed by addition of random hexamer and oligo $(dT)_{18}$ primers (25°C for 15 min) and then primer extension was performed (37°C for 1 h). For each sample, a reaction devoid of reverse transcriptase served as control (Sharma et al., 2017).

Semiquantitative and quantitative PCR to analyze the microRNA expression profile

cDNA was prepared from different human lymphoid cells and mouse tissues, and genomic DNA contamination was checked by performing RT-PCR for house-keeping genes, *HPRT* and/or *18S rRNA*. After normalization of cDNA with respect to *HPRT* and/or *18S rRNA*, semiquantitative RT-PCR was performed using appropriate primers RK65/RK73 for miR-29c-3p to analyze the expression profile of miRNAs in lymphoid cell lines and different mice tissues. PCR products were resolved on 10% native PAGE. Likewise, for quantitative PCR analysis, using the prepared cDNA samples from mouse tissues, and Nalm6 cell line, SYBR green based real time PCR was performed using BioRad IQ5 Real time PCR Detection System Ver2.1 and BioRad CFX96 Touch Real-Time PCR Detection System. *18srRNA* was used as the internal control. Relative expression of miR-29c-3p and RAG1 was analyzed using $2^{-\Delta\Delta Ct}$ method and graph was plotted by subtracting the Ct value of *18S rRNA* from the gene of interest using GraphPad Prism. All reactions were performed in triplicates.

Cloning and sequencing of miRNAs

The PCR amplicon was cut out from native PAGE, crushed into pieces, mixed with 1X TE (Tris-EDTA) and NaCl (500 mM) and incubated at 37°C, (180 rpm, O/N). Glycogen precipitation was done following phenol-chloroform extraction (−20°C for 1 h). Gel purified PCR products were ligated to TA vector (Bangalore Genei, India) using T4 DNA ligase (16°C for 16 h) and transformed into *E. coli DH5α*. Plasmid DNA was extracted, and putative clones were confirmed by restriction digestion with PvuII. Clones of interest were sequenced and analyzed (Medauxin, Bangalore, India).

Pre-miRNA cloning

Pre-miRNA sequence of the selected miRNA was retrieved from the miRBase (Griffiths-Jones, 2004). BLAST was performed with the retrieved pre-miRNA (70-80 nt) sequence against the human genomic DNA. PCR fragment containing pre-miRNA with 200-300 nt upstream and downstream flanking sequence each was PCR amplified from human genomic DNA. The PCR products were resolved on agarose gel (1%), band of interest was cut out and DNA was eluted using gel extraction kit (Sigma-Aldrich, USA) as per manufacturer's instructions. Gel purified PCR products were ligated to the pBluescript (SK+) vector at EcoRV site using T4 DNA ligase (16°C for 16 h) and used for transformation of *E. coli DH5α*. Following blue-white colony selection, clones were screened by restriction digestion with EcoRI and XhoI and confirmed by sequencing. The vector construct was named as pRK3. Further, subcloning of the pre-miRNA sequence of miR-29c was done in the physiological orientation at the site of SalI-SmaI in expression vector pIRES2-EGFP to generate pRK4 and the identity was confirmed by sequencing (Amnion Biosciences, Bangalore, India) Plasmid map was generated using PlasMapper ver 2.0 (Dong et al., 2004).

Quantification of miRNA expression

For the detection of the generation of miR-29c-3p inside the cells upon transfection with the pre-miRNA construct pRK4, total RNA was isolated from Nalm6 cells transfected with different concentration of plasmid DNA (2, 5, 10, and 20 μg), using the TRI reagent

(Sigma-Aldrich: USA) and cDNA was prepared as described above. Presence of genomic DNA contamination was ruled out by DNase treatment followed by RT-PCR of *HPRT* gene. RT-PCR for miR-29c-3p was performed using appropriate gene specific primers RK65/73. *18S rRNA* was used for normalization. The PCR amplified products were resolved on 10% native PAGE. The substrate amount from miRNA and 18S rRNA amplified lanes were quantified and plotted using GraphPad Prism software.

miRNA-mediated regulation of RAG1 expression at different time points

To evaluate the effect of miRNA on the expression of RAG1, the pre-miR-29c construct, pRK4 was transfected into Nalm6 cells by electroporation (300 V, 900 μF, ∞ Ω) and incubated at different time points (24 and 48 h). For electroporation, $3x10^6$ cells were used per transfection. Cells were harvested, washed in PBS (1X), and the cell pellet was resuspended in plain RPMI (400 μl). At the same time, plain RPMI media and pre-miRNA construct were mixed in a volume of 400 μl. Both the samples were mixed, electroporated and resuspended in a volume of 3.2 mL RPMI containing FBS (10%) in six well plates. Cells were harvested after specified time points, extracts were prepared using RIPA buffer (25 mM Tris (pH 7.6), 150 mM NaCl, 1% NP-40, 1% sodium deoxycholate and 0.1% SDS), as described earlier (Kavitha et al., 2009; Sharma et al., 2011). Protein concentration was estimated by Bradford reagent, and samples were equalized on 10% SDS-PAGE.

To evaluate the effect of increasing concentrations of miRNA on the expression of RAGs, increasing concentrations of pRK4 (2, 5, 10, and 20 μg) were transfected into lymphoid cell lines, Nalm6 and Reh by electroporation method as described above. For Nalm6 cells, electroporation parameters used were 300 V, 900 μF, ∞ Ω, while for Reh, it was 250 V, 850 μF, ∞ Ω. Cells were harvested after 48 h, extract was prepared using RIPA buffer method, protein concentration was estimated by Bradford method, and samples were equalized on SDS-PAGE as detailed above.

Immunoblotting

Immunoblotting analysis was performed as described earlier (Chiruvella et al., 2012; Kavitha et al., 2013; Sharma et al., 2015). ~30 μg protein was resolved on 8%–10% SDS-PAGE, transferred to PVDF membrane (Millipore, USA), and blocked with 5% skimmed milk powder for 1 h at room temperature. Membrane was probed with appropriate primary antibodies against RAG1 (1:750), RAG2 (1:750), DICER (3:1000), α-tubulin (1:5000), PCNA (1:3000) and GAPDH (1:750). Blots were washed in PBST (1 X PBS and 0.1% Tween 20) and incubated either with biotinylated secondary antibody or HRP-conjugated antibody (1:10,000) at room temperature for 1 h or at 4° C for 2 h 30 min. The blots were rinsed, incubated with 250 ng/ml streptavidin-HRP (Sigma) for 45 min and washed. The blots were developed using chemiluminescent solution (Immobilon TM western; Millipore, USA) and scanned using gel documentation system (LAS 3000; Fuji, Japan).

Cloning of 3′ UTR of RAG1 containing the seed sequence of miR-29c-3p

3′ UTR sequence of *RAG1* was retrieved from NCBI database and position of seed sequence was mapped by BLAST analysis. A region of 3′ UTR of *RAG1* (4783-5239 nt of human RAG1 mRNA NM_000448.2) containing the seed sequence of miR-29c-3p was PCR amplified using the primers RK84 and RK85 from the human genomic DNA isolated from HEK293T cells. PCR products were resolved on agarose gel (1%), band of interest was cut out and eluted as per the manufacturer's instructions. Purified PCR product was then ligated to the vector pBS (SK+) at the EcoRV or SmaI sites and used for transformation of *E. coli DH5α*. Colonies of interest were selected by blue-white screening, plasmid DNA was isolated and putative clones were screened by digesting with appropriate restriction enzymes. The resulting constructs were named as pRK9 and pRK10, respectively. The insert was then sub-cloned into XhoI-XbaI sites of pmirGLO and EcoRI-NotI sites of pMIR-RECK vectors by directional cloning to ensure that it gets cloned in the physiological orientation. The expression vector constructs were named as pRK17 and pRK12, respectively. Identity of all the clones was confirmed by DNA sequencing.

Site-directed mutagenesis

Mutations were introduced in the seed sequence of miR-29c-3p, which was present on plasmid, pRK9. PCR driven overlap extension methodology was used for inducing site-directed mutagenesis. The primers used for mutagenesis are RK84, RK85, RK90 and RK91. The PCR amplicons harboring the mutations were resolved on agarose gel (1%), band of interest was eluted from agarose gels (Sigma gel elute kit) and cloned into pBS (SK+) at EcoRV site. Colonies were screened by blue-white selection and confirmed by restriction digestion using the enzymes XhoI and XbaI. Identity of the clones were confirmed by sequencing (SciGenom, Cochin). Resulting construct was named as pRK13. Insert DNA harboring the mutation was released by digestion with XhoI and XbaI and ligated into luciferase expression vector, pmirGLO. The construct harboring 3′UTR region of *RAG1* containing the mutant seed sequence of miR-29c-3p was named as pRK15 (Dong et al., 2004).

Luciferase reporter assay

For experimental target gene validations, Nalm6 was transfected with the wild-type *RAG1* 3′UTR-miR-29c-3p (pRK17) or its mutant (pRK15), along with the β-galactosidase vector (Dong et al., 2004). After 48 h of transfection, cells were harvested and lysed in reporter lysis buffer (Promega) and assayed for luciferase activity using luciferase assay reagents (Promega, USA) as per the manufacturer's instructions. The results were normalized for transfection efficiencies against β-galactosidase activity (GLB1 activity). O-nitrophenol β-D galactopyranoside (Hi-Media, India) was utilized for the GLB1 assay (Prabhu et al., 2015).

Transfection studies with anti-miR to evaluate the effect of the miRNA on RAG expression

Nalm6 cells ($5X10^5$) were seeded into 12 well plate, and transfected with increasing concentration of miRNA inhibitor, anti-miR-29c-3p (Invitrogen, USA) (10, 25, 50 and 100 nM) using oligofectamine. Scrambled oligomers (50 nM) were used as control. The cells were harvested after 48 h and cell-free extracts were prepared in RIPA buffer (25 mM Tris (pH 7.6), 150 mM NaCl, 1% NP-40, 1% sodium deoxycholate and 0.1% SDS) as described above. Protein concentration was estimated using Bradford reagent and equalized on SDS-PAGE. The effect due to anti-miR transfection on RAG expression was analyzed by immunoblotting using appropriate antibodies as described above (Sharma et al., 2015).

CRISPR-Cas9 mediated genome editing of miR-29c binding site in RAG1 3'UTR

LentiCRISPRv2 backbone was used to construct CRISPR plasmids containing sgRNA1 and sgRNA2 (Sanjana et al., 2014). LentiCRISPRv2 was digested with BsmBI and the filler fragment was excised. sgRNA1 and 2 were synthesized with overhangs complementary to the BsmBI digested plasmid. The oligomers were ligated to the digested plasmid using T4 DNA ligase and then transformed into bacteria. Identity of the clones were confirmed through sequencing.

HDR construct was generated using pUC19 as backbone. The left-hand homology (LHR) sequence was generated using LHR F1 and R1 primers. The right-hand homology (RHR) sequence was amplified using F2 and RHR R2 primers. The LHR-F1 and RHR-F2 were designed to contain HindIII and XhoI overhangs, respectively. The final sequence was obtained using LHR-F1 and RHR-F2. The primers F1 and R1 were designed to generate mutations at the miR-29c binding site and the PAM sequence. The identity of the construct was confirmed through DNA sequencing.

To study the effect of mutation of the endogenous miR-29c binding site on the *RAG1* 3'UTR, we performed CRISPR-Cas9 mediated genome editing through homologous recombination (Ran et al., 2013). sgRNAs were constructed on pLentiCRISPRv2 backbone which could target the miRNA binding site at the *RAG1* 3'UTR and one upstream. The Pre-B cell line, Nalm6 with Ligase IV mutation and lacking NHEJ was transfected by Polyethyleneimine (PEI) method. Briefly, sgRNA constructs (250, 500 and 1000 ng) along with donor plasmid (250, 500 and 1000 ng) were mixed with linear PEI (DNA: PEI = 1:2) in reduced serum media (Opti-MEM) and incubated at room temperature for 20 min. Plasmid and PEI mixtures were then added onto cells dropwise and incubated at 37° C for 48h. Following this, media was changed and was added along with 0.5 μg/ mL Puromycin for 1 week. The concentration of puromycin was then increased to 1 μg/ mL for over 2 weeks. Genomic DNA was isolated from puromycin resistant clones and sequenced to confirm genomic alteration. Subsequently, immunoblotting, semiquantitative and qPCR was performed with the miR-29c binding site mutated clone B5 to determine the change in RAG1 expression as described above.

In vivo recombination assay

The human lymphoid cell line, Nalm6 was cultured and co-transfected with 3 μg of episomal constructs pGG51 (coding joint) or pGG49 (signal joint) harboring 12 and 23 RSS along with 10 μg of plasmid pRK4 (pre-miR-29c) or pRK12 (*RAG1* 3' UTR) by electroporation (300 V, 900 μF, ∞ Ω) method, and incubated for 72 h at 37° C. The plasmid DNA was recovered using the modified Hirt harvest method and transformed in *E. coli* DH10B (Hirt, 1967; Pattnaik et al., 1993). Mammalian cells were harvested at 72 h post-transfection, spun down at 1200 rpm (4° C, 10 min) and washed with chilled PBS. Cell pellet was resuspended in Hirt buffer (10 mM Tris-HCl pH 8, 10 mM EDTA), SDS (0.06%) was added and mixed gently until cells were lysed. Further, 1 M NaCl was added, mixed gently for 2 min, and incubated overnight at 4° C. The following day, the sample was spun down at 14000 rpm (30 min at 4° C), supernatant was transferred to a new vial, proteinase K (100 μg/ml) was added and incubated for 2 h at 55° C. DNA was purified with phenol:chloroform (1:1) and precipitated by chilled ethanol in the presence of glycogen. DNA pellets were resuspended in 20 μL autoclaved double-distilled water and used for transformation in *E. coli* DH10β by electroporation. The transformation mixture was plated on ampicillin (A) and chloramphenicol-ampicillin (CA) LB agar plates. In brief, recombinant substrates will confer resistance to both antibiotics. The ratio of CA colonies to A colonies reflects the fraction of recovered substrates that underwent V(D)J recombination. Recombination frequency was calculated using the formula (CA/A*100) (Lieber et al., 1988; Raghavan et al., 2001). All experiments were performed in minimum of 3 independent repeats. Change in the recombination efficiency is represented as a bar graph. Statistical significance was calculated using Student's t test with two tailed distribution using GraphPad Prism software. To confirm recombination inside the cells, plasmid DNA was isolated from Ampicillin-Chloramphenicol resistant colonies using alkaline lysis method and analyzed using restriction enzymes AatII-BglII double digestion. Positive clones were sequenced (Amnion Biosciences and Medauxin, Bangalore, India) and analyzed.

Isolation of different stages of B cells using flow cytometry

6-8 weeks old male BALB/c mice were sacrificed. Bone marrow cells were flushed out from femur and tibia and splenocytes were harvested from spleen of three mice per experiment. Both the samples were then filtered using a 40 μm cell strainer. Red blood cells were depicted by a brief hypotonic shock. Cells were then washed once in wash buffer (20 mM HEPES pH 7.4, 2 mM EDTA, 0.5% BSA in 1X PBS and Protease inhibitors) and suspended in blocking buffer (2% FBS, 2% BSA in 1X PBS) for 15 min on ice and washed twice. Cells were then stained using fluorescence tagged antibodies: anti-CD45R-APC, anti-CD43-FITC, anti-CD25-PE-Cy7, anti-IgM-PE Cy7, anti IgD-FITC (BD Biosciences) for 30–45 mins on ice, washed and resuspended in 1X PBS. FACS was performed to isolate three

bone marrow B cell progenitor populations: pro-B cells ($CD45R^+$ $CD43^+$), pre-B cells ($CD45R^+$ $CD25^+$ $CD43^-$), immature B cells ($CD45R^+$ IgM^+) and mature splenic B cells ($CD45R^+$ IgM^- IgD^+) (Zhou et al., 2007). Cell sorting was performed using BD FACSAria II cell sorter.

Analysis of RAG1 expression following Dicer knockdown

shRNA against *DICER1* (TRCN0000290426 and TRCN0000290468) were procured from shRNA Resource Center at Division of Biological Science, IISc, Bangalore (funded by DBT: BT/PR4982/AGR/36/718/2012), Indian Institute of Science (India). To study the effect of Dicer knockdown on expression of RAG1, 5 μg of *DICER1* shRNA construct was transfected into pre-B cell line, Nalm6, by Polyethyleneimine (PEI) method. 5 μg of scrambled plasmid (Scr) was used as the transfection control. For transfection in Nalm6 cells, $5X10^5$ cells were seeded per transfection in RPMI containing 10% FBS. shRNA constructs were mixed with linear PEI (DNA: PEI, 1:2) in reduced serum media (Opti-MEM) and incubated at room temperature for 20 min. Plasmid and PEI mixtures were then added onto cells dropwise and incubated at 37˚C with 5% CO_2. Cells were harvested after 48 h followed by preparation of RIPA extracts. The effect of Dicer knockdown on RAG1 expression was analyzed by immunoblotting using appropriate antibodies as described above (Singh et al., 2019).

Endogenous pulldown of AGO2 using immunoprecipitation assay

4-8 weeks old male C57BL/6 mice were sacrificed. Bone marrow cells were flushed out from femur and tibia of mice and filtered using a 40 μm cell strainer. Red blood cells were depleted by a brief hypotonic shock and the cells were lysed in 1X Cell lysis buffer (50 mM Tris-HCl (pH 8), 150 mM NaCl, 2 mM $MgCl_2$, 0.5% Triton X, 2 mM EDTA + Protease inhibitors) for 1 h at 4˚C. The lysate was incubated with Protein A/G Sepharose beads bound to anti-Ago2 antibody (3 μg) at 4˚C on rotation for 7 h. Anti-rabbit IgG was used as the secondary control. After washing the beads twice with 1X PBS, TRI reagent (Sigma-Aldrich; USA) was added to the beads. RNA isolation and preparation of cDNA was performed using adaptor primers for miR-29c-3p as described earlier. PCR amplification using gene specific primers, RK65/73 and RK10/S83 for miR-29c-3p and RAG1, respectively was carried out. The PCR amplified products were resolved on 10% Native PAGE.

Argonaute HITS-CLIP to determine miR-29c interaction with RAG1 3' UTR

AGO-HITS CLIP using datasets from a prostate cancer cell line 22rv1 was performed to determine miR-29c interaction with RAG1 3'UTR. Browser viewable genomic bigWig files and expression count files from the 22rv1 HITS-CLIP experiment (GEO: GSE137071) were uploaded onto the Integrated Genomics Viewer (IGV), and the genomic locations for miR-29c-3p and RAG1 were checked for signals (Fernandes et al., 2021). IGV is a genome browser that supports visualization of locations of genomic experiments, where the browser compatible files (bigWig and expression count files in this case) can be loaded as tracks, corresponding to the respective genomes and viewed/analyzed for presence of a binding signal (Robinson et al., 2011).

QUANTIFICATION AND STATISTICAL ANALYSIS

Flow cytometry data were analyzed using BD FACS DIVA software version 6.1.3. Immunoblots and gels were analyzed and quantified with Multigauge software. Statistical analyses were performed using one-way ANNOVA or Student's t test by comparing multiple conditions with control sample set using GraphPad Prism 5.0 or 7.0 (GraphPad Software). The statistical details of experiments are presented in the relevant figure legends. A p value of < 0.05 was considered significant.